



Turun yliopisto
University of Turku

A large, stylized green graphic of a hand with fingers spread, positioned on the left side of the cover. The hand is rendered in a flat, modern style with a dark green outline and a lighter green fill. The fingers are slightly curved, and the palm is visible. The background is a solid green color.

DETERMINING THE SIZE OF RETINAL FEATURES: A STUDY ON THE MAGNIFICATION OF A FUNDUS PHOTOGRAPH AND ITS APPLICATION IN THE DEVELOPMENT OF REACTION TIME PERIMETRY

Laura Knaapi



Turun yliopisto
University of Turku

**DETERMINING THE SIZE OF
RETINAL FEATURES: A STUDY ON
THE MAGNIFICATION OF A FUNDUS
PHOTOGRAPH AND ITS APPLICATION
IN THE DEVELOPMENT OF REACTION
TIME PERIMETRY**

Laura Knaapi

University of Turku

Faculty of Medicine
Institute of Clinical Medicine
Department of Ophthalmology
Doctoral Programme in Clinical Research

Supervised by

Professor Eija Vesti, M.D., Ph.D.
Department of Ophthalmology
University of Turku
Turku, Finland

Dr. Markku Leinonen, M.D., Ph.D.
Ocuspecto Ltd
Turku, Finland

Reviewed by

Adjunct Professor Olavi Pärssinen, M.D., Ph.D.
Department of Ophthalmology
University of Jyväskylä
Jyväskylä, Finland

Associate Professor Juha Toivonen, Ph.D.
Tampere University of Technology
Tampere, Finland

Opponent

Professor Tero Kivelä, M.D., Ph.D.
Department of Ophthalmology
University of Helsinki
Helsinki, Finland

The originality of this thesis has been checked in accordance with the University of Turku quality assurance system using the Turnitin OriginalityCheck service.

ISBN 978-951-29-7307-1 (PRINT)

ISBN 978-951-29-7308-8 (PDF)

ISSN 0355-9483 (PRINT)

ISSN 2343-3213 (PDF)

Painosalama Oy – Turku, Finland 2018

To Jonni

ABSTRACT

Determining the Size of Retinal Features: a Study on the Magnification of a Fundus Photograph and its Application in the Development of Reaction Time Perimetry

University of Turku, Faculty of Medicine, Institute of Clinical Medicine,
Department of Ophthalmology, Doctoral Programme in Clinical Research, Turku, Finland
Annales Universitatis Turkuensis, Medica-Odontologica, 2018, Turku, Finland

Painosalama Oy – Turku, Finland 2018

Fundus photography plays a vital part in the diagnosis and follow-up of ocular pathology. Both the camera optics and the ametropia of the given eye influence the magnification of a fundus photograph. Determining the true size of retinal features thus requires the use of mathematical equations.

This study was aimed at evaluating the formula of Bennett et al. (1994) for determining the size of retinal features in two different clinical settings. First, its use was verified with healthy volunteers by measuring the macula-disc center distance from fundus photographs taken with the telecentric Zeiss fundus camera, and by calculating the theoretical location of the blind spot based on the macula-disc center distance. These results were compared with the results from a visual field examination using the Octopus custom made Blind Spot visual field program. The theoretical location of the blind spot, derived from calculations based on fundus photography, corresponded to the visual field examination derived location of the physiological blind spot. In addition, the magnification characteristics of the Topcon fundus camera were assessed by calculating its conversion factor.

Secondly, the accuracy of the formula was evaluated after cataract surgery and IOL implantation. Cataract surgery and IOL implantation did not have an effect of clinical significance on the magnification of a fundus photograph taken with the telecentric Zeiss and Topcon fundus cameras even after the ametropia and the anterior chamber depth were changed due to surgery.

Thirdly, the use of the macula-disc center distance as a reference tool for determining the size of retinal features from fundus photographs was evaluated in prematurely born children aged from 10 to 11 years. The macula-disc center distance was found to be close to a constant.

Lastly, a novel method for examining the visual field was introduced. Reaction time perimetry was shown to be able to detect the physiological blind spot. The location of the blind spot was verified with two independent methods: First, by calculating the theoretical location of the blind spot based on the macula-disc center distance derived from fundus photographs taken with the telecentric Zeiss fundus camera, and second, by visual field examination using the Octopus custom made Blind Spot visual field program. Validating the use of reaction time perimetry in different ocular pathology requires further studies.

Keywords: retinal feature, fundus photography, blind spot, macula-disc center distance, reaction time perimetry

TIIVISTELMÄ

Verkkokalvon rakenteiden koon määrittäminen silmänpohjan valokuvauksen avulla ja reaktio-aikaan perustuvan näkökenttätutkimuksen kehittäminen

Turun yliopisto, Lääketieteellinen tiedekunta, Silmätautioppi, Turun kliininen tohtori-ohjelma

Annales Universitatis Turkuensis, Medica-Odontologica, 2018, Turku, Finland

Painosalama Oy – Turku, Finland 2018

Silmänpohjan valokuvauksella on tärkeä merkitys silmänpohjan sairauksien seurannassa. Sekä kameran optiikalla että silmän taittovoimalla on vaikutus silmänpohjan valokuvan suurennokseen. Objektin todellisen koon määrittäminen silmänpohjan valokuvasta vaatii näin ollen matemaattisten kaavojen käyttöä.

Tämän väitöskirjan tavoitteena oli tutkia Bennettin ym. vuonna 1994 kehittämää matemaattista kaavaa verkkokalvon rakenteiden koon arvioimiseksi. Kaavan käyttö verifioitiin käytännössä terveillä vapaaehtoisilla koehenkilöillä mittaamalla tarkan näön alueen ja näköhermon pään keskipisteiden välimatka silmänpohjan valokuvista, jotka oli otettu Zeissin telesentrisellä silmänpohjan valokuvauskameralla. Kuvien perusteella laskettiin sokean täplän teoreettinen sijainti. Saatujen tulosten todettiin vastaavan Octopus-näkökenttätutkimuksen avulla määritetyn fysiologisen sokean täplän sijaintia. Lisäksi tutkimuksessa laskettiin Topconin silmänpohjan valokuvauskameran muuntokerroin.

Kaihileikkauksessa keinomykiön asentamisella aiheutetun silmän taittovoiman ja etukammion syvyyden muuttumisella ei todettu olevan kliinisesti merkittävää vaikutusta Zeissin telesentrisellä eikä Topconin silmänpohjan valokuvauskameralla otettujen silmänpohjan valokuvien suurennokseen.

Tutkimuksessa selvitettiin myös keskosuuden vaikutusta tarkan näön alueen ja näköhermonpään keskipisteiden välimatkaan. Välimatkan todettiin olevan lähellä vakiota 10–11 -vuotiailla keskosena syntyneillä lapsilla. Näin ollen johtopäätöksenä oli, että sitä voitaisiin käyttää referenssinä keskosena syntyneillä henkilöillä, kun silmänpohjan valokuvasta halutaan määrittää objektin koko.

Lopuksi tutkimuksessa esiteltiin uusi reaktioajan mittaukseen perustuva menetelmä, jonka avulla voidaan tutkia näkökenttää. Reaktioajan mittaukseen perustuvan näkökenttälaitteen todettiin löytävän sokean täplän terveillä vapaaehtoisilla. Tulos verifioitiin määrittämällä sokean täplän sijainti kahden muun menetelmän avulla: selvittämällä sen teoreettinen sijainti Zeissin silmänpohjan valokuvauskameralla otettujen silmänpohjan valokuvien perusteella ja tutkimalla fysiologisen sokean täplän sijainti Octopus-näkökenttätutkimuksen avulla. Reaktioajan mittaukseen perustuvan menetelmän soveltuvuus näkökentän tutkimiseen terveillä vapaaehtoisilla ja eri silmänsairauksien yhteydessä vaatii kuitenkin jatkotutkimuksia.

Avainsanat: verkkokalvon rakenne, silmänpohjan valokuvaus, sokea täplä, tarkan näön alueen ja näköhermonpään keskipisteiden välimatka, reaktioajan mittaukseen perustuva näkökentän tutkiminen

TABLE OF CONTENTS

ABSTRACT	4
TIIVISTELMÄ	5
LIST OF ORIGINAL PUBLICATIONS (I–IV)	8
ABBREVIATIONS	9
1 INTRODUCTION	10
2 REVIEW OF THE LITERATURE	12
2.1 Selection of basic optical principles.....	12
2.1.1 Snell’s law.....	12
2.1.2 Small-angle approximation.....	12
2.1.3 Nodal points.....	13
2.1.4 Focal points and planes.....	13
2.1.5 Principal points and planes	14
2.1.6 Modeling an unknown optical system	15
2.2 The Schematic eye of Gullstrand.....	17
2.3 Magnification characteristics of fundus cameras.....	17
2.3.1 General principles of fundus cameras.....	17
2.3.2 Telecentric lenses.....	18
2.3.3 The Zeiss fundus camera	18
2.3.4 The Topcon fundus camera.....	20
2.4 Determining the size of a retinal feature by fundus photography	21
2.5 The reliability of the formula of Bennett et al. (1994) compared to other methods for calculating the true size of a retinal feature	24
2.6 Macula-disc center distance	24
2.7 Testing algorithms in standard automated perimetry	25
2.8 Limitations and challenges of standard automated perimetry.....	25
2.9 Reaction time as a marker for visual processing speed.....	26
3 AIMS OF THE THESIS	27
4 SUBJECTS AND METHODS	28
4.1 Subjects (I–IV).....	28
4.2 Fundus photography (I–IV).....	29
4.3 Clinical examination (I–IV).....	30
4.4 Calculations carried out on fundus photographs.....	30
4.4.1 Determining the magnification of digitalization of fundus photographs taken with the Zeiss fundus camera (I)	30

4.4.2	Calculating the conversion factor of the Topcon fundus camera (I and II)	32
4.4.3	Calculating the macula-disc center distance (I, III and IV), the dimensions of the optic disc (III), and the distance between the two retinal vessel crossings (II) in mm	32
4.4.4	Calculating the surgery induced change in the location of the second principal point P' (II)	33
4.5	Determining the location of the blind spot with Octopus (I and IV)	33
4.6	Calculating the theoretical location of the blind spot (I and IV).....	35
4.7	Reaction time perimetry (IV)	35
4.8	Statistical analyses (I–IV)	37
5	RESULTS.....	38
5.1	The conversion factor of the Topcon fundus camera (I and II).....	38
5.2	Macula-disc center distance (I, III and IV)	38
5.3	Dimension of the optic disc (III)	38
5.4	Correlation of relative change in the measured distance between two retinal vessel crossings with preoperative axial length, change in ametropia in D, and change in the anterior chamber depth in mm (II)	39
5.5	Theoretical versus physiological location of the blind spot (I)	39
5.6	Reaction times within and outside of the blind spot area in reaction time perimetry (IV)	42
6	DISCUSSION	43
6.1	Determining the size of retinal features (I and II)	43
6.2	The conversion factor of the Topcon fundus camera (I and II).....	45
6.3	Macula-disc center distance (I and III)	46
6.4	Reaction time perimetry (IV)	48
7	SUMMARY AND CONCLUSIONS.....	50
8	FUTURE DIRECTIONS	51
8.1	The use of the formula of Bennett et al. (1994) after cataract surgery and IOL implantation (II).....	51
8.2	Reaction time perimetry (IV)	51
9	ACKNOWLEDGEMENTS.....	52
10	RERERENCES.....	53
	ORIGINAL PUBLICATIONS	57

LIST OF ORIGINAL PUBLICATIONS (I–IV)

This thesis is based on the following publications, which are referred in the text by Roman numerals I–IV.

- I Knaapi L, Aarnisalo E, Vesti E & Leinonen MT (2015): Clinical verification of the formula of Bennett et al. (1994) of determining the size of retinal features by fundus photography. *Acta Ophthalmol* **93**: 248–252.
- II Knaapi L, Lehtonen T & Vesti E (2017): The effect of cataract surgery and IOL implantation on the magnification of a fundus photograph: a pilot study. *Acta Ophthalmol* **95**: 839–841.
- III Knaapi L, Lehtonen T, Vesti E, Leinonen MT (2015): Determining the size of retinal features in prematurely born children by fundus photography. *Acta Ophthalmol* **93**: 339–341.
- IV Knaapi L, Vesti E, Leinonen MT (2015): Detecting the Physiological Blind Spot with Reaction Time Perimeter. *J Clin Exp Ophthalmol* **6**:493. doi:10.4172/2155-9570.1000493

The original publications have been reproduced with permission of the copyright holder.

ABBREVIATIONS

D	Diopters
ETMK	Eettinen toimikunta
FO	Fixation object
HRA+OCT	Heidelberg Retina Angiography + Optical Coherence Tomography
IBM	International Business Machines Corporation
IOL	Intraocular lens
ODF	Optic-Disc-to-Fovea Distance
RNFL	Retinal nerve fiber layer
ROP	Retinopathy of prematurity
SAP	Standard automated perimetry
SD	Standard deviation
SD-OCT	Spectral Domain Optical Coherence Tomography
SPSS	Statistical Package for the Social Sciences
STS	Saccade triggering stimulus

1 INTRODUCTION

Fundus photography is of vital importance in the diagnosis and follow-up of ocular pathology. Both the camera optics and the ametropia of the given eye influence the magnification of a fundus photograph (Bengtsson & Krakau 1992, Bennett et al. 1994, Littmann 1982). Hence, mathematical equations are needed to determine the size of retinal features.

Over twenty years ago, Bennett et al. (1994) published their formula for calculating the true size of a retinal feature from fundus photographs taken with a telecentric fundus camera. In their article, Bennett et al. (1994) noted the fact that all formulas have experimental and inherent errors, and that their formula is not an exception.

The formula of Bennett et al. (1994) applies to fundus photographs taken with the telecentric Zeiss fundus camera. The magnification characteristics of the Zeiss fundus camera have previously been presented in detail (Bengtsson & Krakau 1977, Rudnicka et al. 1998). However, such specific information is not available on all cameras used for fundus photography.

When a fundus photograph of unknown magnification has been taken, it is necessary to rely on other ways to determine the size of the object of interest. Different means have been invented in order to investigate the magnification characteristics of the Topcon fundus camera (Meyer & Howland 2001; Quigley & Dubé 2003). Bartling et al. (2008) showed that the macula-disc center distance can be used as a reference tool when measuring the size of the optic disc and other retinal parameters on digital fundus photographs taken with different cameras with an unknown magnification factor.

In this thesis one of the primary objective was to evaluate the reliability of the formula of Bennett et al. (1994) in two different clinical settings. First, this was done by measuring the macula-disc center distance from fundus photographs taken with the telecentric Zeiss fundus camera and by calculating the theoretical location of the blind spot based on the macula-disc center distance using healthy volunteers. These results were compared with the results from a visual field examination using the Octopus custom made Blind Spot visual field program through which the location of the physiological blind spot was determined. Secondly, the accuracy of the formula was evaluated after cataract surgery and IOL implantation.

In addition, the objective of this thesis was to study the effect of prematurity on the macula-disc center distance, and to evaluate whether it can be used as a reference tool for measuring the size of an object from a fundus photograph taken from prematurely

born children aged from 10 to 11 years. Lastly, the aim was to validate a novel method for detecting the location of the physiological blind spot, namely reaction time perimetry.

2 REVIEW OF THE LITERATURE

2.1 Selection of basic optical principles

2.1.1 Snell's law

According to Snell's law, which was named after its discoverer, a refracted ray lies in the same plane as the incident ray and the surface normal (Figure 1). Snell's law states that

$$n_1 \cdot \sin \theta_i = n_2 \cdot \sin \theta_t$$

where n_1 and n_2 represent the refractive index of incident and transmitted medium, respectively. θ_i and θ_t represent the angle of incidence and transmission, respectively. (Clinical Optics 2005–2006, p. 46.)

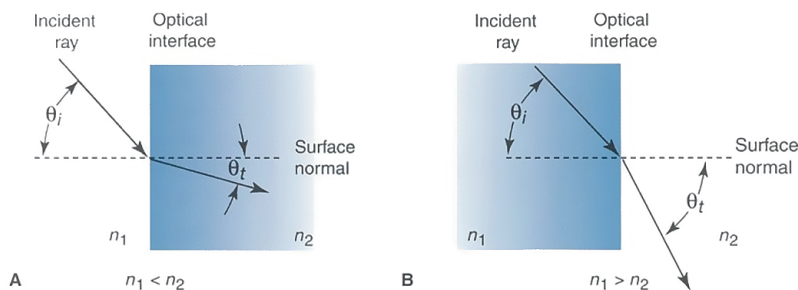


Figure 1. The angle of transmission is smaller than the angle of incidence when the refractive index of the transmitted medium is higher than the refractive index of incident medium and vice versa. Adapted from Clinical Optics 2005–2006, p. 46, Figure 2-25.

2.1.2 Small-angle approximation

A ray that is close to the optical axis over its entire path is called a paraxial ray. Snell's law has to be applied in order to determine the direction of the refracted ray. The sine function can be expressed as

$$\sin \theta = \theta - \theta^3/3! + \theta^5/5! - \theta^7/7! \dots$$

Here θ is expressed in radians.

When the angle θ is small as in small-angle or paraxial approximation, only θ becomes significant and every term after it can be taken as 0. Hence, the previous equation can be expressed as

$$\sin \theta = \theta$$

In small-angle approximation, Snell's law can be expressed as

$$n_1 \cdot \theta_i = n_2 \cdot \theta_t$$

where θ is expressed in radians. (Clinical Optics 2005–2006, p. 59.)

2.1.3 Nodal points

The anterior and posterior nodal points (N and N', respectively) of an optical system have a specific property: from any object point, a ray can be found that passes through the anterior nodal point and continues its path emerging from the optical system along the line connecting the posterior nodal point and the image point (Figure 2). The two angles that are formed by these lines and the optical axis are equal thus following the relationship:

$$\text{image height} / \text{image distance} = \text{object height} / \text{object distance}$$

The two nodal points coincide in the center of the lens when a simple thin lens is situated in a uniform medium such as air or water. (Clinical Optics 2005–2006, p. 31–32.)

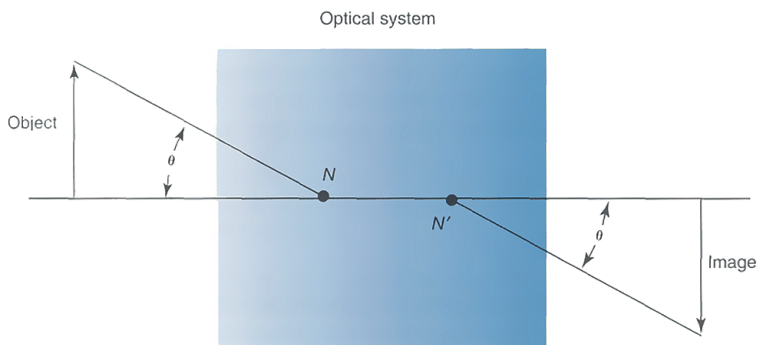


Figure 2. The essential property of the nodal points is that the angle (θ) formed by a ray traveling from an object point to the anterior nodal point and the optical axis is equal to the angle (θ) formed by a ray traveling from the posterior nodal point to an image point and the optical axis. Adapted from Clinical Optics 2005–2006, p. 31, Figure 2-8.

2.1.4 Focal points and planes

The location of the anterior focal point F (in meters) – situated in front of a plus lens – can be calculated by $1 / D$, where D represents the power of a given lens in diopters (Figure 3 A). In a plus lens all rays emanating from F_a or the anterior focal plane form a narrow beam and come to focus at plus optical infinity (Figure 3 B). The opposite is true for rays of a narrow beam entering a lens from minus infinity: they focus to the posterior focal point F_p situated posterior to a plus lens (Figure 3 C). For a minus lens the focal points are reversed in such a way that the F_a is located posterior and the F_p anterior to the lens. Light rays that leave the object at a same angle will cross at the posterior focal plane (Figure 3 D). (Clinical Optics 2005–2006, p. 69–71.)

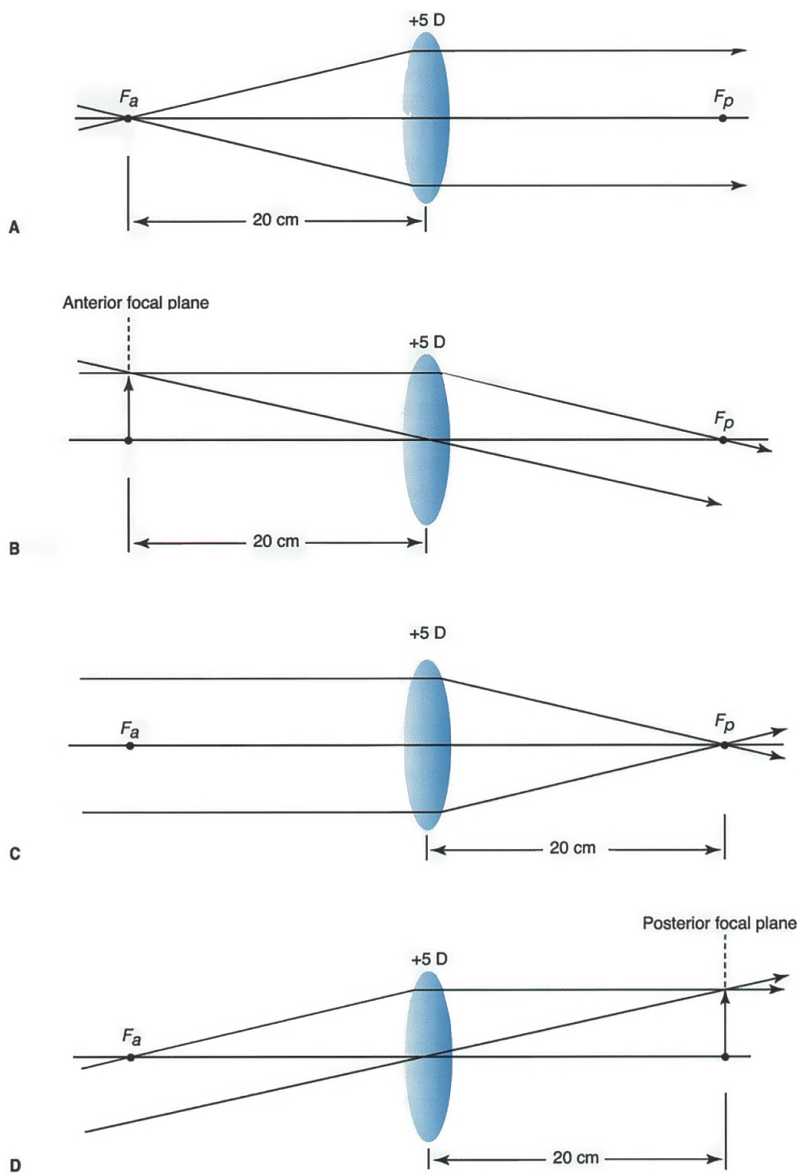


Figure 3. Rays that travel through the anterior focal point and the plus lens form a narrow beam (A). Rays from the anterior focal plane focus to plus optical infinity (B). Rays from minus optical infinity that are parallel with the optical axis focus to the posterior focal point (C). Rays from minus optical infinity not parallel with the optical axis focus to the posterior focal plane (D). Adapted from *Clinical Optics 2005–2006*, p. 70, Figure 2-48.

2.1.5 Principal points and planes

In a thick lens, all of the refraction appears to take place at the anterior and posterior principal planes. In a thick lens a ray that travels through the lens and emerges from the back of the lens appears to have crossed the posterior principal plane at the same

distance from the optical axis as the incident ray coming from in front of the lens appears to have crossed the anterior principal plane from the optical axis. In other words, the incident rays appear to converge toward the anterior principal plane P and form a virtual object. The emerging rays appear to emanate from a virtual image at posterior principal plane P'. The virtual object and the virtual image located at the anterior and posterior principal planes, respectively, are of the same size. (<http://ecee.colorado.edu/~mcleod/pdfs/OESD/lecturenotes/ThickLenses.pdf>.)

In an optical system comprised of many lenses, if the object is located at the anterior principal plane, the image will be formed at the posterior principal plane. The image will be real, oriented upright, and of the same size as the object. Therefore the anterior and posterior principal planes are also known as the planes of unit magnification. (Clinical Optics 2005–2006, p. 75–76.)

The anterior and posterior principal planes are perpendicular to the optical axis and their point of intersection with the optical axis forms the location of the anterior and posterior principal points P and P', respectively (Clinical Optics 2005–2006, p. 76). If the media on both sides of the lens are uniform and have the same refractive indexes, the principal points coincide with the nodal points (Figure 4 E).

The two principal points, together with the focal and nodal points, form a group of points called *the cardinal points* (Clinical Optics 2005–2006, p. 76). Together they determine the location, orientation and the size of an image.

2.1.6 Modeling an unknown optical system

The human eye, like many other complex optical systems, is comprised of multiple refracting surfaces (Figure 4 A). The cardinal points and planes can be used to approximate and simplify their magnification characteristics. However, the optical surfaces must be spherical and the analysis restricted to paraxial rays. In complex optical systems comprised of multiple lenses the location of the cardinal points and planes can be determined experimentally by using a laser pointer. (Clinical Optics 2005–2006, p. 76–78.)

The anterior focal point F_a can be determined by detecting the intersection of a ray of light from an object point with the optical axis where the ray of exit is parallel to the optical axis. Furthermore, the intersection of entering and exiting rays determines the location of the anterior principal plane P. (Figure 4 B.)

When another ray of light from the same object point travels parallel to the optical axis, it can be used to define the posterior focal point F_p by detecting the location of intersection of the exiting ray with the optical axis. The crossing of the entering and

exiting rays in this case determines the location of the posterior principal plane P' . (Figure 4 C.)

The points where the entering and exiting rays intersect the optical axis at the same angle are defined as the nodal points (Figure 4 D). These points overlap the principal points when the optical system is surrounded by media of the same refractive indexes (Figure 4 E).

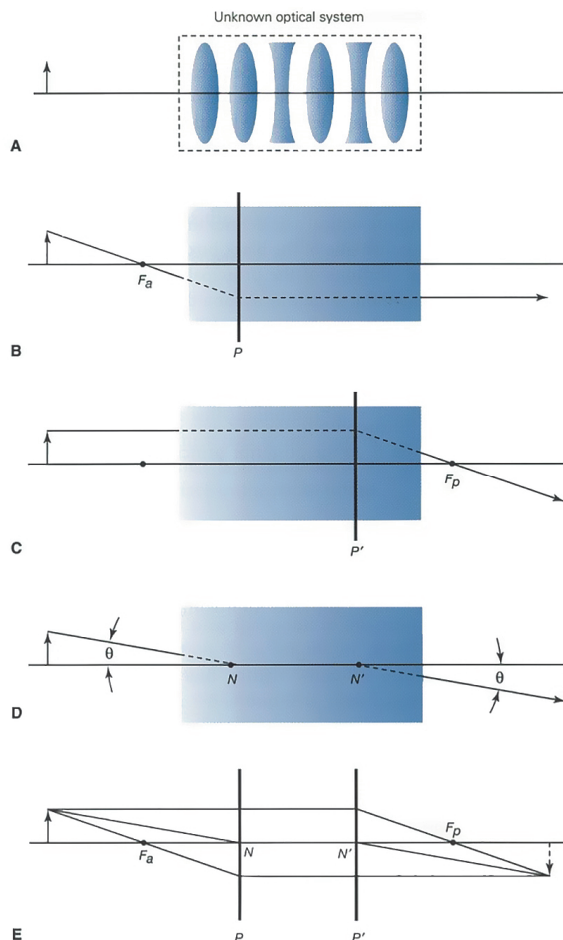


Figure 4. (A) An unknown optical system is comprised of many lenses of varying power. (B) A ray of light from the object that travels through the anterior focal point continues parallel to the optical axis after refraction by the optical system. These entering and leaving rays intersect at the anterior principal plane P . (C) A light ray leaving the object parallel to the optical axis will cross with the optical axis at the posterior focal point after refraction by the optical system. These two rays intersect at the posterior principal plane P' . (D) Entering and exiting rays form the same angle (θ) with the optical axis at the anterior and posterior nodal points. (E) The cardinal points and planes form a simplified model of an unknown optical system. In this example, the refractive indexes of the bounding media on both sides of the optical system are equal, thus causing the nodal points to correspond to the principal points. Adapted from *Clinical Optics 2005–2006*, p. 77, Figure 2-55.

2.2 The Schematic eye of Gullstrand

In 1911, Gullstrand, a Swedish professor of ophthalmology, won the Nobel prize for a schematic eye that closely approximated the human eye. Other mathematical models of the eye's complex optical system have been developed, e.g., by Listing, Donders, Tscherning, von Helmholtz and others. (Clinical Optics 2005–2006, p. 105.)

Figure 5 shows the positions of the cardinal points used for optical calculations in Gullstrand's model. Differences between the various models have been studied by De Almeida & Carvalho (2007) and Bakaraju et al. (2008).

The so called *Reduced Schematic eye* makes even further simplifications compared to Gullstrand's model. In it, the two principal and nodal points of the cornea and the lens are substituted with a single intermediate point, respectively. This enables the eye to be treated as a single refracting element, a spherical surface, that is separated by two different media with two different refractive indexes (1.0 for air and 1.33 for the eye). However, because all models include simplifications and approximations, they only partially conform to reality. In the optics of the human eye biology plays a vital part, and can cause aberrations and irregularities, thus causing a lack of mathematical certainty. (Clinical Optics 2005–2006, p. 105–106.)

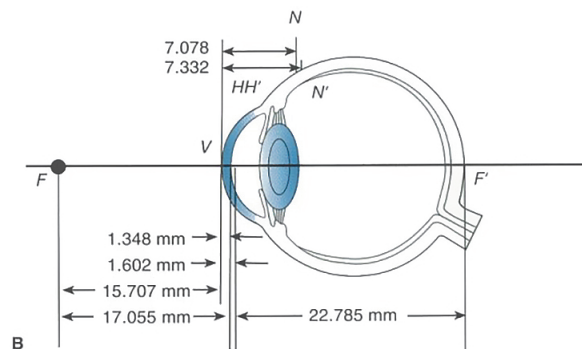


Figure 5. In Gullstrand's schematic eye the cardinal points are located as above. Here **HH'** stands for the anterior and posterior principal points. **N** designates the anterior and **N'** the posterior nodal point. **V** is corneal vertex. **F** and **F'** are the anterior and posterior focal points, respectively. Adapted from Clinical Optics 2005–2006, p. 106, Figure 3-1.

2.3 Magnification characteristics of fundus cameras

2.3.1 General principles of fundus cameras

In fundus cameras two different light sources are used: one is for illuminating the subject's eye and the other – a flash lamp – produces a bright flash used for

photography. The condensing lens of the camera is a part of the camera's optical system nearest to the eye and produces an "aerial" image. The camera lens then focuses on this image and projects it further onto photographic film or an image sensor plane. (Clinical Optics 2005–2006, p. 275–279.)

2.3.2 Telecentric lenses

Nontelecentric lenses produce several problems affecting measurement accuracy and repeatability. With nontelecentric lenses the magnification of the image changes if the location of the object changes. In addition, image distortion, perspective errors, poor image resolution and object edge position uncertainty may arise. These difficulties can be reduced and sometimes even cancelled with the help of telecentric lenses. (<http://www.opto-engineering.com/resources/telecentric-lenses-tutorial>.)

With the use of object-space telecentric lenses the image size will not change even when the location of the object changes as long as the object is within a limit called "the telecentric range". This is possible by placing a stop aperture on the front focal plane of the lens. Thus, only the ray cones that have a principal ray parallel to the optical axis are allowed to travel through the aperture. (<http://www.opto-engineering.com/resources/telecentric-lenses-tutorial>.)

With image-space telecentric lenses the principal rays that leave the lens are parallel to the optical axis and hit the film or image sensor at a zero angle of incidence. Hence, focusing of the lens is possible at different distances while leaving the size of the image unchanged. (<http://www.opto-engineering.com/resources/telecentric-lenses-tutorial>.)

2.3.3 The Zeiss fundus camera

The Zeiss fundus camera designed by Littmann was presented to the German Ophthalmological Society in 1955 (Littmann 1955). Behrendt & Doyle (1965) found that errors of exposure, camera positioning, and changes in focusing did not affect the quantitative measurements carried out on fundus photographs taken with the Zeiss fundus camera. However, large defocusing did make measurements uncertain due to blurring of the margins of the structures in question. Differences in the centering of the image on the negative resulted in errors up to 10 %.

The findings of Pach et al. (1989) were that varying the distance between the eye and the camera had no notable effect on the size of an optic disc image in an emmetropic eye. On the contrary in high ametropia the magnification of the Zeiss fundus camera depends on the camera-to-eye distance according to Lotmar (1984). In his work, Lotmar (1984) presented an example of an eye with ametropia of + 16 D. Change in

the magnification was 1.6 % per one mm of variation in the camera-to-eye distance. He discusses the fact that magnification differences of several percent can occur in cases of high ametropia because a ± 2 mm difference in the camera-to-eye distance does not affect image quality considerably. In addition, according to Lotmar (1984) changing the camera's diopter range scales for ametropia also has an impact on the magnification of approximately 5 %. Arnold et al. (1993) reported a change in the magnification from -4.5 % to +6.8 % in myopic conditions, and from -5.6% to +4.6 % in hyperopic conditions, when the camera-to-eye distance was changed by ± 5 mm. Their study was conducted using a model eye.

The findings of Pach et al. (1989) were that decentration of the disc image resulted in a 2% increase in image size per one mm of eccentricity. Artificial refractive ametropia induced in one subject with soft contact lenses from + 8.00 D to -8.00 D had no effect on the magnification. Furthermore, no statistically significant difference was found in the size of the images of optic discs between subjects who had varying degrees of refractive ametropia, aphakia or axial ametropia up to 3 D.

The essential features of the telecentric principle of the Zeiss fundus camera have been thoroughly explained in the work of Bengtsson & Krakau (1977) and in the works of Bennett et al. (1994) and Rudnicka et al. (1998). The following is a summary of the basic features illustrated in Figure 6 adapted from Rudnicka et al. (1998):

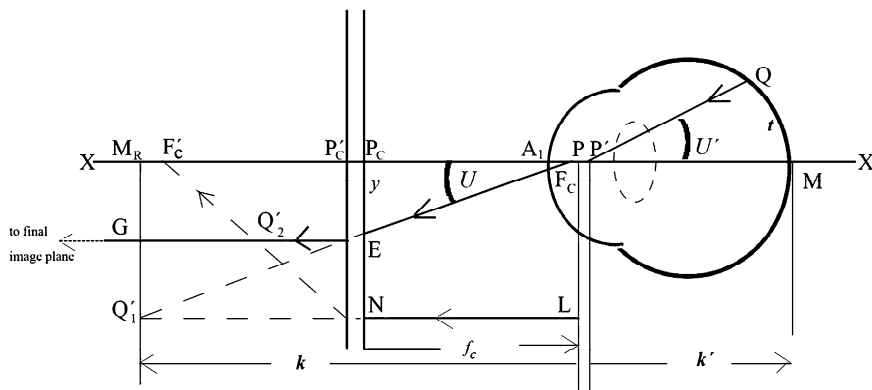


Figure 6. The camera components of a telecentric imaging system nearest the subject's eye are represented as a thick lens and its anterior and posterior principal points denoted with P_c and P'_c , respectively. The ray PE becomes parallel with the optical axis of the camera after refraction by this lens. The size of the image on the camera film plane is directly proportional to the distance y . In a telecentric optical system the final image is at infinity, which causes the ratio of the image size on the camera film plane to the distance y to be a constant over a wide range of ametropia. Figure adapted from Rudnicka et al. (1998).

In Figure 6, the two principal points of the eye are marked with P and P'. A₁ indicates the corneal vertex. The distance from P to the eye's far point plane M_R is marked with k and k' is the distance from P' to the retina. The anterior focal length of the camera is f_c . Q represents a point on the retina and gives rise to the ray QP'. The distance between Q and M is t . The camera's optical components nearest the subject's eye are illustrated here with a single thick lens with its anterior and posterior principal points with P_c and P'_c, respectively. The camera's anterior principal focus F_c and the eye's anterior principal point P are made coincident. The refracted ray PE is derived from QP', and forms the angle U with the optical axis. After refraction by the camera's imaging system, the refracted ray PE becomes parallel with the optical axis, and the ray EG will emerge. The distance P_cE is equal to y . In a telecentric fundus camera the image size on the camera film or image sensor plane is directly proportional to y over a wide range of ametropia. The distance y is determined by the angle U , which in turn is proportional to U' .

On refraction by the eye itself an image Q'₁ will be formed on the eye's far point plane M_R. In myopia M_R is located in the front of the eye and in hyperopia behind the retina. Q'₁ is located on the path of the refracted ray PE. It follows that Q'₁ will then become an object for the camera's imaging system and a second image Q'₂ will be formed. Its location can be found as follows: A ray from NL will be refracted to F'_c, i.e., the posterior focal point of the camera's imaging system. The place where this ray crosses the emergent ray EG designates the location of Q'₂. Ray EG is parallel to the optical axis and continues its way to the camera's film or image sensor plane.

2.3.4 The Topcon fundus camera

Meyer and Howland (2001) found that the results of mean optic disc areas of different racial groups analyzed with various machines including the Topcon fundus camera differed compared to those taken with the Zeiss fundus camera. They then calculated a multiplier which was called a normalizing factor for the Topcon and found it to be 1.04 compared to the Zeiss fundus camera. The normalizing factor for the Zeiss fundus camera was considered to be 1 by definition.

Quigley and Dubé (2003) introduced a method for estimating the true size of a retinal object from a fundus photograph taken with two different Topcon fundus cameras (TRC-50F and TRC-50X; Topcon American Corp). The distance of the objective lens from the film plane is altered in order to bring the image into focus with a focusing knob. The position of the knob was registered against a fixed point on the camera body with a 180 degree protractor or by a photocopy of a 150 mm ruler attached on the knob. Their results showed that the position of the knob correlated highly with the refractive error of the given eye. Thus, an additional step where the refractive error of

the eye is determined by other means, was no longer needed. However, in this method, the eye-camera magnification still needs to be calculated with a proper formula based on the refractive error of the given eye.

2.4 Determining the size of a retinal feature by fundus photography

In Littmann's formula

$$t = 1.37 \cdot q \cdot s \quad (\text{Equation 1})$$

This formula is used for determining the true size of a retinal feature from a fundus photograph taken with the telecentric Zeiss fundus camera (Littmann 1982). Here t stands for the true size of a retinal feature, the constant 1.37 ($^{\circ}/\text{mm}$ over the range of ametropia from -16 to +17 D) applies to the telecentric Zeiss fundus camera used by Littmann, q ($\text{mm}/^{\circ}$) is determined by the optical dimensions of the given eye, and s equals the size of a retinal feature on the camera film. The quotient q ($\text{mm}/^{\circ}$) can be determined from nomograms published by Littmann (1982). Factors required for reading the value of q from these nomograms are ametropia and the anterior corneal radius.

Coleman et al. (1996) studied two cynomolgus monkeys (*Macaca fascicularis*) and placed retinal tacks of known size near their optic discs. They found that Littmann's nomograms gave a good estimation of the true size of an image on film taken with the telecentric Zeiss fundus camera if the eye's dimensions fall within the range of Littmann's nomograms.

Bennett et al. (1994) further developed the formula of Littmann (1982) into the form of:

$$t = 0.01306 \cdot (x - 1.82) \cdot 1.37 \cdot s \quad (\text{Equation 2})$$

In the formula of Bennett et al. (1994) Littmann's q is replaced by $0.01306 \cdot (x - 1.82)$. This is derived from the following (Bennett et al. 1994; Rudnicka et al. 1998):

The radian measure of U' can be taken as

$$U' = t / k' \quad (\text{Equation 3})$$

when t is very small (Figure 6).

Furthermore, according to small-angle approximation

$$U' = U / n \quad (\text{Equation 4})$$

where $n = 1.336$ and represents the refractive index of the final ocular medium.

Hence, the size of a given object t on the retina can be expressed by

$$t = k' \cdot U' = k' \cdot U / n \quad (\text{Equation 5; } U \text{ in radians})$$

From the relationship between degrees and radians it follows

$$U'^{\circ} / 360^{\circ} = t / (2 \cdot \pi \cdot k') \quad (\text{Equation 6; } U'^{\circ} \text{ in degrees})$$

and

$$t = (2 \cdot \pi \cdot k') \cdot U'^{\circ} / 360^{\circ} = k' \cdot U'^{\circ} \cdot (\pi / 180^{\circ}) = k' \cdot U^{\circ} / n \cdot (1 / 57.296^{\circ}) \quad (\text{Equation 7})$$

where $n = 1.336$.

Thus,

$$t = k' \cdot U^{\circ} / 76.547^{\circ} = 0.01306 / ^{\circ} \cdot k' \cdot U^{\circ} \quad (\text{Equation 8})$$

According to the telecentric system

$$s = U^{\circ} / p \quad (\text{Equation 9})$$

where U° is expressed in degrees and p is a constant for the particular fundus camera used.

Thus,

$$t = 0.01306 \cdot k' \cdot s \cdot p \quad (\text{Equation 10})$$

The Equation 10 corresponds to Littmann's original formula $t = 1.37 \cdot q \cdot s$ (Littmann 1982). The constant p equals 1.37 ($^{\circ}/\text{mm}$) and is specific to the Zeiss fundus camera used by Littmann. Littmann's q is replaced by $0.01306 \cdot k'$ in the formula of Bennett et al. (1994).

According to Bennett et al. (1994), even though k' cannot be determined directly, it can be closely approximated. This can be done by subtracting the mathematical location of the second principal point P' from the apex of the cornea, i.e., by subtracting 1.82 mm from axial length x . This leads to the final form of the formula

$$t = 0.01306 \cdot (x - 1.82) \cdot 1.37 \cdot s \quad (\text{Equation 11})$$

The mathematical location of the second principal point P' of a given eye is subject to varying forces depending on the power and the location of the crystalline lens and the cornea (Bennett et al. 1994). Hence, in reality the constant 1.82 is different between individuals and could be subject to change (Bennett et al. 1994).

Bennett et al. (1994) postulated that individual variations in P' are unlikely to exceed ± 0.55 mm. This would result in the following change in the formula:

$$t = 0.01306 \cdot (x - 1.82 \pm 0.55) \cdot 1.37 \cdot s \quad (\text{Equation 12})$$

In total this would result in a maximum error of only

$$0.01306 \cdot (\pm 0.55) = \pm 0.007 \quad (\text{Equation 13})$$

in q .

However, according to Rudnicka et al. (1998), when a nontelecentric fundus camera is used, additional information is needed since the camera constant p in the formula of Bennett et al. (1994) will no longer be a single constant value but will vary depending on the refraction of the given eye. Information concerning the camera constant p for particular instruments was not readily available (personal communication with both Topcon Corporation, Tokyo, Japan and Canon Inc., Tokyo, Japan).

In their work, Rudnicka et al. (1998) represented a means to calculate p for a nontelecentric fundus camera, such as a Canon, based on the ocular refraction of a given eye. They analyzed the magnification properties of 11 different fundus cameras using a previously published model eye (Rudnicka et al. 1992). All but one of the different Zeiss fundus cameras studied were found to be of a telecentric design and to have a constant magnification factor. In contrast, all models of the Canon fundus camera were nontelecentric and exhibited a linear relationship between the magnification factor of the camera and ametropia. The equations representing this linear relationship were calculated for all the nontelecentric cameras studied (Rudnicka et al. 1998).

Rudnicka et al. (1998) discussed the fact that the magnification factor of a nontelecentric camera should be calculated using the correct equation and by substituting the patient's ocular refraction at the corneal vertex into the equation. Ocular refraction at the corneal vertex can be calculated using another equation where the ocular refraction at the corneal vertex R and spectacle ametropia A are expressed in diopters, and d is the vertex distance in meters: $R = A / (1 - d \cdot A)$.

In addition, Rudnicka et al. (1998) found that the magnification factors of nontelecentric fundus cameras not only vary between different models, but also the degree of variation is different between various cameras. It can potentially lead to considerable error if an incorrect camera magnification factor is used when calculating the size of an object from a fundus photograph. Therefore, the correct magnification factor should be chosen for the precise camera. This is especially important in the case of high ametropia.

2.5 The reliability of the formula of Bennett et al. (1994) compared to other methods for calculating the true size of a retinal feature

In their work, Bennett et al. (1994) represented the optical constants of the personalized schematic eyes of 12 individuals. The constant 1.82 mm, which is accepted as the general value of P' , i.e., the location of the second principal point from the apex of the cornea in their formula, was compared to the true values of P' of these 12 eyes. The true values of P' were within the limit of 1.70 mm to 2.26 mm. Accepting 1.82 mm as the general value of P' was thus considered to be reliable by Bennett et al. (1994).

Garway-Heath et al. (1998) compared different methods of evaluating the size of a retinal feature. In addition, they identified their sources of error. The method that uses the most biometric data, namely information concerning axial length, anterior chamber depth, crystalline lens thickness, keratometry, and ametropia, also presented by Bennett et al. (1994), was considered to be the benchmark. All other methods, including the formula of Bennett et al. (1994) where 1.82 mm is accepted as the general value of P' , were compared to this method. The other methods evaluated, and which are presented by different authors, all use various biometric data: ametropia and keratometry only (Bengtsson & Krakau 1992; Littmann 1982; Wilms 1986), axial length (Bengtsson & Krakau 1992; Bennett et al. 1994; Littmann 1988; Wilms 1986) and ametropia only (Bengtsson & Krakau 1992). In addition to these, a new method was presented and evaluated by Garway-Heath et al. (1998) as well as a method that uses Heidelberg retina tomography. Both of these methods use biometric information concerning keratometry and ametropia.

The results of Garway-Heath et al. (1998) showed that when the axial length is known the formula of Bennett et al. (1994) gives results that are close to the method that uses most biometric data. It is superior in accuracy compared to the methods that use information based on keratometry and ametropia alone. Hence, if the axial length is known, Garway-Heath et al. (1998) recommend the use of the formula of Bennett et al. (1994) instead of those methods. They also discussed the various sources of error of the different methods. All the methods rely on biometric data derived from measurements carried out in order to determine the different optical components of the eye. Therefore, they all are subject to measurement error regardless of the accuracy of the theoretical basis of the methods themselves (Garway-Heath et al. 1998).

2.6 Macula-disc center distance

The macula-disc center distance has been found to be close to a constant in adults (Bartling et al. 2008; Hong et al. 2010; Mok & Lee 2002). Hence, it represents an internal reference tool that can be used for determining the size of retinal features on

fundus photographs taken with nontelecentric fundus cameras or when the optical principals of the particular camera used are not known (Bartling et al. 2008).

2.7 Testing algorithms in standard automated perimetry

Testing algorithms in standard automated perimetry (SAP) are divided into different test groups. In suprathreshold tests a bright stimulus above the expected normal threshold values is presented in different locations of the visual field. The quantitative sensitivity to light is not determined. These algorithms are used for screening. (Kanski & Kubicka-Trzaska 2007, p. 26; Yanoff & Duker 2009, p. 1128.)

In 2-level screening strategy a stimulus having an intensity of 4 dB below the normal sensitivity threshold is presented at each location examined. When this stimulus is seen, the location is considered to have normal sensitivity and given a + sign. When this stimulus is not seen, another stimulus of maximal intensity that the perimeter can present is shown at the same location. If the second stimulus is not seen, the location is marked with a black box which represents an absolute scotoma. If the second stimulus is seen, the location is marked with a white box and represents a relative scotoma. (Racette et al. 2016, p. 94–95.)

In threshold testing, the threshold values are determined by detecting the amount of light that can be dimmed from the maximal intensity (10 000 apostilbs in Humphrey perimetry) and still be detected 50 % of the time. For this purpose, a staircase method is used where the intensity of a stimulus is changed by steps that represent a 4 dB increase in the intensity of a stimulus until a threshold is crossed. After this the intensity is decreased by 2 dB steps thus reaffirming the threshold. Hence, threshold testing is a quantitative assessment, and can be used for monitoring glaucomatous field defects. (Kanski & Kubicka-Trzaska 2007, p. 26-27; Yanoff & Duker 2009, p. 1128.)

2.8 Limitations and challenges of standard automated perimetry

Visual field defects can be quantified by SAP (Kanski & Kubicka-Trzaska 2007, p. 27). The connection between visual field defects and the ability to perform the activities of daily living have been studied by Richman et al. (2010) and McKean-Cowdin et al. (2007).

An external fixation control apparatus is needed in standard automated perimetry because fixation losses can occur and they potentially weaken the reliability of the study (Katz & Sommer 1988). It has been discussed that for children the most demanding requirement for automated visual field examination is to maintain a stable fixation on a central target while at the same time paying attention to peripheral stimuli (Tschopp et al. 1998).

2.9 Reaction time as a marker for visual processing speed

The ability to move the eyes towards an object perceived in the peripheral visual field in order to fixate with the fovea is a fundamental feature of the visual system. Visual processing speed, which is defined as the time needed to make a correct judgment about a visual stimulus, has been studied by measuring reaction times (Tatham et al. 2014).

3 AIMS OF THE THESIS

The primary objectives of the thesis were

1. To clinically verify the formula of Bennett et al. (1994) for determining the size of retinal features by measuring the macula-disc center distance from fundus photographs taken with the telecentric Zeiss fundus camera, and then by calculating the theoretical location of the blind spot based on the macula-disc center distance. These results were compared to the location of the physiological blind spot determined by the Octopus custom made Blind Spot visual field program. Furthermore, the purpose was to study the magnification characteristics of the Topcon fundus camera.
2. To study the effect of change in ametropia and anterior chamber depth caused by cataract surgery and IOL implantation on the magnification of a fundus photograph taken with the telecentric Zeiss and Topcon fundus cameras.
3. To study the effect of prematurity on the macula-disc center distance and to evaluate whether it could be used as a reference tool for calculating the size of retinal features from fundus photographs in prematurely born children aged from 10 to 11 years.
4. To study the ability of a novel reaction time perimeter to detect a physiological scotoma, i.e., the blind spot.

4 SUBJECTS AND METHODS

4.1 Subjects (I–IV)

The participants in Study I were 17 healthy volunteers aged 22 – 44 years who were recruited based on their various ocular refraction. They underwent fundus photography at the Turku University Hospital. Eleven of these 17 subjects were included in Study IV. Of the total of 17 participants, 13 underwent visual field analysis in Study I and 11 in Study IV by methods later to be explained in 4.5 and 4.7.

In Study I, the ocular refraction of all the 17 participants varied from -7.88 to +3.63 D (spherical equivalent) and of the remaining 11 participants in Study IV from -7.88 to -0.50 D. Maximum astigmatism was 1.75 D in both studies. The mean axial length of all the 17 participants was 24.13 mm, SD 1.51. Intraocular pressure was within 10 and 21 mmHg. The left eye was chosen to be analyzed.

In Study II, 11 volunteers aged 44 – 89 years undergoing cataract surgery at Turku University Hospital were recruited based on their various ocular refraction. They underwent fundus photography preoperatively and approximately one month after surgery. The right eye was chosen to be examined. Nine subjects returned for the postoperative follow-up visit and were included in the analyses.

In Study II, the pre and postoperative ocular refraction (spherical equivalent) was from -21.38 to + 3.25 D and from -3.50 to -0.25 D, respectively. The average change in ocular refraction induced by cataract surgery and IOL implantation was +3.52 D, SD 6.86. The mean axial length was 25.11 mm, SD 1.95 (range from 21.18 to 28.02 mm). Intraocular pressure was within 10 and 21 mmHg.

Different systemic or ocular pathology was not considered to be a part of the exclusion criteria in Study II. However, none of the subjects had undergone previous ocular surgery which could have altered the ametropia of the eye and thus the magnification of a fundus photograph.

In Study III, fundus photographs taken from 27 prematurely born children aged from 10 to 11 years were analyzed. These subjects were originally recruited for another study. The median gestational age at birth was 30 weeks (range from 23 to 36 weeks) and the median birth weight was 1260 g (range from 525 to 1905 g). The ocular refraction varied from +4.50 to -20.50 D (spherical equivalent) and astigmatism was up to 1.00 D. The mean axial length was 23.01 mm, SD 0.78. In this study, intraocular pressure was not measured.

In Study III, one child (subject 20) had had ROP (stage 3+ in both eyes) that had required laser treatment. Subject 20, was an outlier, and therefore, was removed from

all the analyses and calculations of the mean values. The results of subject 20 were presented as a case report. The axial length of subject 20 was 25.64 mm. Three other children had been diagnosed with strabismus and one with anterior uveitis. The left eye was chosen to be analyzed.

Informed written consent was given by all the participants in Studies I, II and IV or by their parents and legal guardians in Study III after an explanation of the nature and possible consequences of the study. This was done according to the Finnish Ethics committee of Turku University Hospital (ETMK 52/180/2012). All research adhered to the tenets of the Declaration of Helsinki.

4.2 Fundus photography (I–IV)

Fundus photography was performed with the telecentric Zeiss (FF-4; Carl Zeiss Meditec, Jena, Germany) in all studies except Study III, and with the Topcon fundus camera (TRC-50DX; a 50 degree lens) in all studies but IV. All images were analyzed digitally using the ImageJ -program (version 1.4.3.67, <http://imagej.nih.gov/ij/>).

The macula-disc center distance in both Studies I and IV was determined from digital fundus photographs based on a method presented by Hong et al. in 2010 (Figure 7). At least one fundus photograph taken with both the telecentric Zeiss and Topcon fundus cameras showed both the macula and the optic disc and was in focus. Therefore no one was excluded based on this criterion.

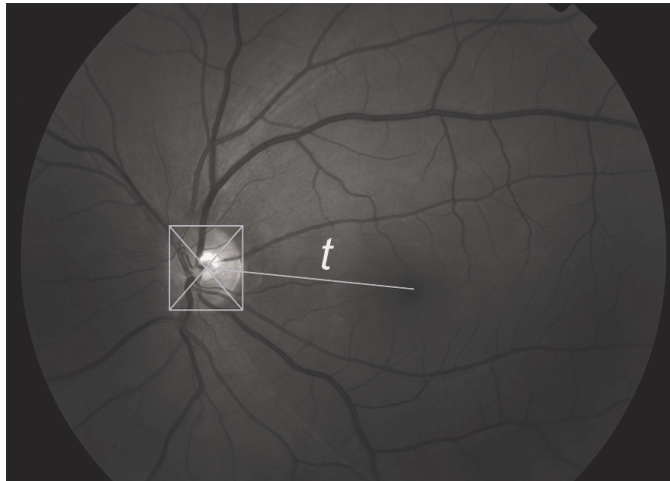


Figure 7. Measuring the macula-disc center distance (t) from a fundus photograph. A rectangle was positioned around the border of the optic disc. The center of the rectangle was determined by drawing two lines from the top to the bottom corners of the rectangle thus determining the center of the rectangle. The macula-disc center distance was calculated from the center of the macula to the center of the rectangle. Adapted from Study I.

A subject was not enrolled in Study II if a fundus photograph taken with the telecentric Zeiss (FF-4; Carl Zeiss Meditec, Jena, Germany) and Topcon fundus cameras (TRC-50DX; a 50 degree lens) before and approximately one month after surgery did not show the same two distinct fundus landmarks, i.e., two retinal vessel crossings. No one was excluded based on this criterion.

The macula-disc center distance in Study III was measured in the same way as in Studies I and IV. In addition, the width and the height of the optic discs were measured. At least one fundus photograph taken with the Topcon fundus camera showed both the macula and the optic disc and was in focus. Therefore no one was excluded based on this criterion.

4.3 Clinical examination (I–IV)

The ocular refraction of each eye was determined using streak retinoscopy in Studies I, III and IV and autorefractometry (NIDEK ARK-1s, Nidek Co., LTD.) in Study II. Intraocular pressure was measured using the Icare tonometer (TA01i, Icare Finland Oy) in all studies but III. Fundus examination was done with slit lamp biomicroscopy (BQ-900; Haag-Streit, Bern, Switzerland) and a +90 diopter lens in all studies. The axial length in all studies and the anterior chamber depth in Study II was determined using the IOL-Master (Carl Zeiss Meditec, Jena, Germany).

4.4 Calculations carried out on fundus photographs

4.4.1 Determining the magnification of digitalization of fundus photographs taken with the Zeiss fundus camera (I)

In order to use the formula of Bennett et al. (1994) the size of an object on film s has to be determined. This poses a problem to be solved since the object on the film is very small. With the use of telecentric digital fundus cameras this problem is no longer an issue, since a computer program can be used in order to calculate the true size of a given object on a digital fundus photograph (personal communication with Carl Zeiss Meditec, Jena, Germany). Furthermore, when a computer program is not available, with the help of the knowledge of the size of one pixel on the image sensor of a telecentric digital camera in mm, the size of the object of interest can be measured in pixels from a digital photograph and then this knowledge used in order to calculate its size in mm on the image sensor. This corresponds to s in the formula of Bennett et al. (1994).

In Studies I, II and IV the telecentric Zeiss fundus camera used had a film camera attached, and the following procedure was used to determine s :

A piece of millimeter paper was placed at the posterior focal point of a +10 D lens (Bengtsson & Krakau 1992) using a special object and lens holder designed by the author with the help of Mr. Kari Nummelin and the personnel working at the technical support of Turku University Hospital who also constructed the device (Figure 8).



Figure 8. Two lens holders separated from an old piece of trial frames were attached to a long screw with the help of two white plastic circles. These circles possessed a pair of holes in the middle of them. The first hole in the middle of the anterior plastic circle closest to the camera on the left side of the figure allowed light from the camera to travel through. The hole in the middle of the posterior plastic circle was unnecessary. The anterior plastic circle on the left was attached to a metal plate that also had a hole in the middle through which light from the camera could travel. The metal plate was held in place by two metal bars located between the head and chin rests of the camera with the help of two cable ties. A +10 D lens was placed in the anterior lens holder. Then a piece of millimeter paper (not shown in the figure) was attached on the front surface of another lens placed in the posterior lens holder on the right side of the figure. The posterior lens holder attached to the posterior plastic circle could be moved back and forth along the screw by pressing a small black button underneath the plastic circle. By this means the piece of millimeter paper on top of a lens in the posterior lens holder was placed 10 cm behind the anterior + 10 D lens. Adapted from Study I.

The piece of millimeter paper placed at the posterior focal point of a +10 D lens was photographed with the telecentric Zeiss fundus camera using the special object and lens holder. The true size of one millimeter of the photographed millimeter paper on film was determined by attaching another piece of millimeter paper on the bottom corner of the film and by taking a photograph of the film with a digital camera and a slide duplicator. By this means a digital image of the film with an image of the original millimeter paper taken with the telecentric Zeiss fundus camera and another piece of millimeter paper attached to it was obtained. This obtained image was then magnified on a 46-inch television screen. The ratio of one mm of the photographed millimeter paper on the film

and one mm of the millimeter paper attached to it was then calculated. The result was 0.43388. By this means, the true size of one mm of the millimeter paper originally photographed with the telecentric Zeiss fundus camera was obtained.

Furthermore, the same piece of film with an image of the millimeter paper photographed with the telecentric Zeiss fundus camera was digitalized in the same way as were all the fundus photographs taken with the telecentric Zeiss fundus camera at a local photographic retailer. From this digital image of the original millimeter paper photographed with the telecentric Zeiss fundus camera the size of one mm of the photographed millimeter paper in pixels was calculated (23.05 pixels = 1 digital mm). With the help of the knowledge of the true size of one mm of the millimeter paper on film (one photographed mm on film was 0.43388 mm), the ratio of one pixel/mm was calculated (23.05 pixels/0.43388 mm = 53.13 pixel/mm). In this way, the size of one mm of the millimeter paper on film converted to a digital photograph could be measured in pixels and then calculated in true mm on film.

4.4.2 Calculating the conversion factor of the Topcon fundus camera (I and II)

In Study I, the conversion factor of the Topcon fundus camera (mean 194.98 pixel/mm) was determined by calculating the ratio of the macula-disc center distance in pixels measured from fundus photographs taken with the Topcon fundus camera and the corresponding distance in mm derived from calculations carried out on fundus photographs taken with the telecentric Zeiss fundus camera using the results from all the 17 healthy volunteers. The conversion factor derived from these calculations was also used in Study III.

In Study II, the pre and postoperative conversion factors of the Topcon fundus camera were calculated. This was done by first measuring the distance between the same two retinal vessel crossings in pixels from pre and postoperative fundus photographs taken with the Topcon. These results were then divided with the corresponding distances in mm derived from calculations carried out on pre and postoperative fundus photographs taken with the telecentric Zeiss fundus camera. Furthermore, any surgery induced relative change in the conversion factors was calculated.

4.4.3 Calculating the macula-disc center distance (I, III and IV), the dimensions of the optic disc (III), and the distance between the two retinal vessel crossings (II) in mm

The true size of the macula-disc center distance (corresponding to t in the formula of Bennett et al. 1994) was calculated in mm from fundus photographs taken with the Zeiss fundus camera using the formula of Bennett et al. (1994) in Studies I and IV. In

Study III, the size of the macula-disc center distance was determined from fundus photographs taken with the Topcon fundus camera using the calculated conversion factor of the Topcon (194.98 pixel/mm). In addition, in Study III the dimensions of the optic disc were determined using the same conversion factor.

In Study II, the distance between two retinal vessel crossings was calculated from fundus photographs taken with the telecentric Zeiss fundus camera before and approximately one month after surgery using the formula of Bennett et al. (1994). The pre and postoperatively measured axial length was used in the calculations carried out on fundus photographs taken before and after surgery, respectively.

4.4.4 Calculating the surgery induced change in the location of the second principal point P' (II)

Surgery induced change in the mathematical location of the second principal point of the eye P' was calculated in Study II. Here two assumptions had to be made: The first assumption was that the preoperative mathematical location of P' was equal to 1.82 mm (Bennett et al. 1994). The second assumption was that the true size of the preoperatively calculated distance between two retinal vessel crossings was correct. The postoperative location of P' was calculated based on these assumptions by substituting the calculated preoperative distance in the place of the variable t , and the corresponding measured postoperative distance in the place of the variable s in the formula of Bennett et al. (1994).

4.5 Determining the location of the blind spot with Octopus (I and IV)

The location of the physiological blind spot of the left eye was determined using Octopus (Octopus 900; Haag-Streit, Bern, Switzerland), and a custom made Blind Spot visual field program using a one degree oval grid of 139 test points covering the expected location of the physiological blind spot in Studies I and IV. Using a 2-level screening strategy and a Goldmann III (4 mm²) size stimulus the program was designed to search the expected area of the blind spot (from 9° to 20° temporal).

A test point with an absolute defect was considered to belong to the blind spot. The obtained results were rounded to the nearest half degree and compared with the theoretical location of the blind spot calculated from fundus photographs taken with the telecentric Zeiss fundus camera.

At this point, subject 1 was excluded from further calculations in Study I because the Octopus custom made Blind Spot visual field analysis showed only a relative scotoma in the blind spot area. Repeating the test resulted in poor fixation. However, after careful evaluation, the results of subject 1 were included in Study IV together with the

results of 10 other subjects who had also participated in Study I. The reason for this was that the reliability factor of the initial Octopus custom made Blind Spot visual field analysis of subject 1 was 0 even though it showed only a relative scotoma. In addition, the location of the center of the theoretical blind spot of subject 1 (15.2°) corresponded to the location of the center of the physiological blind spot (15.5°). Furthermore, light scattering is known to cause the area of the blind spot to not be totally blind (Meyer et al. 1997) and this was thought to possibly have influenced the results of subject 1.

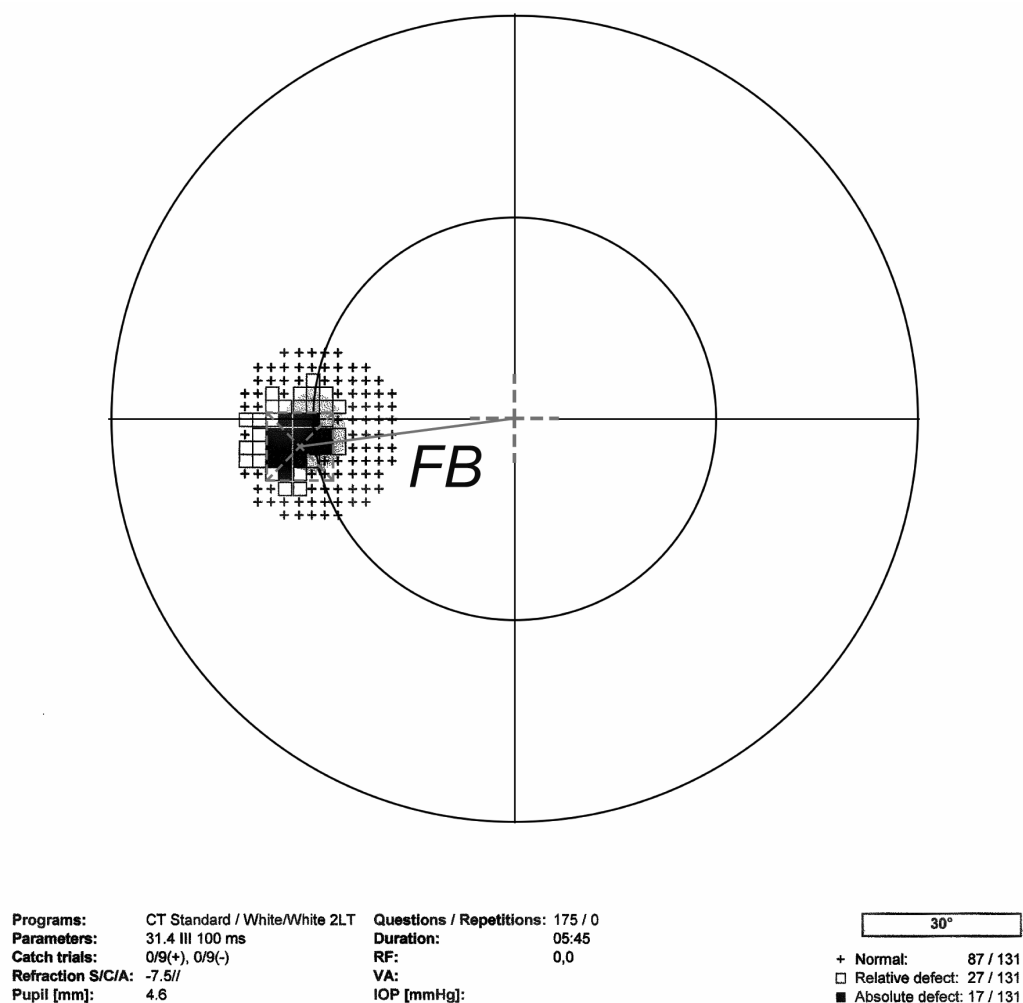


Figure 9. Normal output of the visual field examination with the Octopus perimeter using the custom made Blind Spot visual field program. The black circles represent 15° and 30° eccentricity and the black boxes mark the absolute scotoma area, i.e., the blind spot. The center of the blind spot was calculated using a similar method as described in Fig 7. FB is the distance between the fixation point and the center of the blind spot in degrees. Adapted from Study I.

4.6 Calculating the theoretical location of the blind spot (I and IV)

The macula-disc center distance in degrees (U') was closely approximated using geometry (Figure 10):

$$U' = (t \cdot 360^\circ) / (2 \cdot \pi \cdot (x - 1.82)) \quad (\text{Equation 14})$$

The macula-disc center distance in degrees (U') was then multiplied with the refractive index of the final ocular medium ($n = 1.336$) in order to calculate the theoretical location of the blind spot (Figure 10).

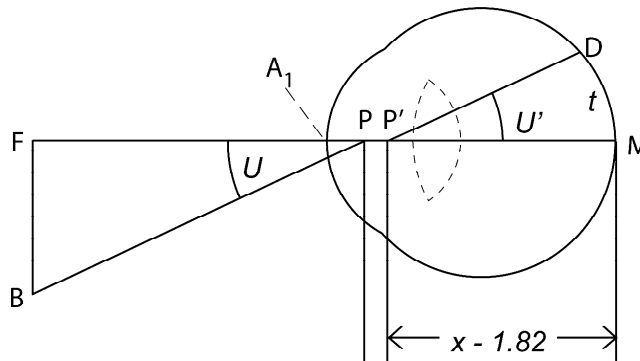


Figure 10. Calculating the theoretical location of the blind spot in degrees (U). The distance between the center of the macula (M) and the center of the optic disc (D) is marked with t . U' represents the macula-disc center distance in degrees. P stands for the first and P' for the second principal point of the eye. F is the fixation point and B the blind spot in the visual field. $U' = U / n$, where $n = 1.336$ and stands for the refractive index of the final ocular medium. $x - A_1P' = x - 1.82$, where x is the axial length and 1.82 the location of the second principal point of the eye from the apex of the cornea. Adapted from Bennett et al. (1994).

4.7 Reaction time perimetry (IV)

A microcontroller driven reaction time perimeter (Ocuspecto Ltd, Turku, Finland) comprised of a 35° arc (radius 54 cm) was constructed including 15 LEDs (diameter 0.6 mm) compiled in six 3×5 arrays for displaying both the STS (Saccade triggering stimulus) and the FO (Fixation object). The STS, which was nearly equivalent to the stimulus size of Goldmann III (diameter 0.4° with the viewing distance of 54 cm), was formed with a flash of an array of 3×3 LEDs lasting for 100 ms. Viewing distances of 54 cm and 48 cm were used and checked with a measuring tape. The absolute size of the STS in mm^2 did not change with different viewing distances. The size of the STS in degrees at the viewing distance of 48 cm was approximately 0.5° . Hence, change in the size of the STS in degrees was considered to be insignificant.

A single STS was immediately followed by an arrow head figure pointing either to the right or left serving as the FO (Figure 11). Recognition of the FO was reported by the subject by pressing the correct button on a remote control (right or left, respectively). By this means fixation with the fovea was verified. The intensity of the FO was only from 3 to 5 dB above the individually predetermined visibility threshold of the arrow in order to prevent parafoveal recognition of the FO. This threshold was determined beforehand by increasing the arrow brightness beginning from zero until the subject could recognize it. After correct recognition of the FO a new peripheral STS followed by another FO was immediately displayed at a different location of the visual field in order to initiate a reflex saccade towards the STS. Time intervals between button presses were recorded.



Figure 11. The reaction time perimeter showing six visual stimulus units (large openings in the aluminum arc) that were constructed with 3x5 LED arrays and assembled on a printed circuit board. These were capable of displaying the Saccade triggering stimuli (size Goldmann III) and an arrow head figure (< or >; see the inset picture) which represented the Fixation object. The small opening in the center of the aluminum arc is for an ambient light sensor used for measuring the intensity of room lighting. The remote control (not in the picture) for reporting the recognition of the Fixation object is connected to the perimeter by cable. Data transfer to a computer was done after the test using a USB cable. Adapted from Study IV.

Eighteen locations, up to 28° temporal and 20° nasal (-27.7°, -25°, -20°, -18°, -16.6°, -15°, -13.3°, -12°, -11.1°, -10°, +10°, +11.1°, +12°, +13.3°, +15°, +16.6°, +18°, +20°) along the meridian 8° of the visual field of the left eye, were tested from three to six times. This meridian was chosen as it allowed more locations to be tested within the blind spot area than meridian 0°. The reaction time perimeter had an electronic sensor with which

the correct tilt for studying the chosen meridian 8° was adjusted. The visual field program did not proceed if the tilt changed. This did not occur at all during the study.

The number of locations that were situated within the blind spot area varied from 3 to 5 (mean 3.5) and depended on the location of the individual's physiological blind spot. In this study, the location of the blind spot was defined as the center of the blind spot determined by the Octopus custom made Blind Spot visual field program $\pm 2.5^\circ$. Reaction times for detecting the STS displayed within the blind spot area were compared to reaction times at other locations. The study time depended on the reaction times of a given individual and varied between 1 and 2 minutes for both distances.

4.8 Statistical analyses (I–IV)

The IBM SPSS Statistics v 21 software package was used for statistical analyses. In Study I, the normality of the parameters was tested using the Kolmogorov-Smirnov Test. Pearson correlation coefficients were calculated in order to test correlation between ametropia and the macula-disc center distance as well as between ametropia and the conversion factor of the Topcon fundus camera. A Bland-Altman plot (Bland & Altman 1986) was used to compare the method for calculating the location of the theoretical blind spot and the method for determining the location of the physiological blind spot.

In Study II, in order to test correlation between relative change in the measured distance between two retinal vessel crossings and the preoperative axial length, change in ametropia in D, and change in the anterior chamber depth in mm before and after surgery, Pearson correlation coefficients were calculated using the IBM SPSS Statistics v. 21 software package. The normality of the parameters was tested using the Kolmogorov-Smirnov Test. Furthermore, correlation between surgery induced relative change in the conversion factor of the Topcon fundus camera and preoperative axial length, change in ametropia in D, and change in the anterior chamber depth in mm was tested by calculating Pearson correlation coefficients.

In Study III, correlation between ametropia and the macula-disc center distance was tested by calculating the Pearson correlation coefficient using the IBM SPSS Statistics v. 21 software package. The normality of the parameters was tested using the Kolmogorov-Smirnov Test. Subject 20, who was an outlier, was removed from these analyses.

In Study IV, the reaction times within the blind spot area of all the individuals were compared to the reaction times in other locations in the visual field. Statistical analysis was carried out using the Analysis of Variance (AOV) procedure of the IBM SPSS Statistics v. 22 software package.

5 RESULTS

5.1 The conversion factor of the Topcon fundus camera (I and II)

In Study I, the mean conversion factor of the Topcon fundus camera for a 50 degree lens of all the 17 subject analyzed was 194.98 pixel/mm, SD 10.40 and 75.70 pixel/degree, SD 2.55. Correlation was found between the conversion factor of the Topcon fundus camera and ametropia (Pearson correlation coefficient, $r = 0.70$, $p < 0.01$).

In Study II, the mean pre and postoperative conversion factors of the Topcon fundus camera for a 50 degree lens were 185.47 pixel/mm, SD 12.36 and 183.27 pixel/mm, SD 13.92. The average surgery induced relative change in the conversion factor of the Topcon fundus camera was -1.19%, SD 0.03. No statistically significant correlation was found between relative change in the conversion factor of the Topcon fundus camera and change in ametropia in D (Pearson correlation coefficient, $r = -0.17$, $p = 0.66$). Furthermore, neither change in the anterior chamber depth in mm nor preoperative axial length correlated significantly with relative change in the conversion factor of the Topcon fundus camera (Pearson correlation coefficient, $r = -0.41$ and -0.30 , $p = 0.28$ and 0.44 respectively).

5.2 Macula-disc center distance (I, III and IV)

In Study I, the mean macula-disc center distance of all the 17 participants was 4.73 mm, SD 0.29. The corresponding mean macula-disc center distance in degrees was 12.18°, SD 0.74. No statistically significant correlation was found between ametropia and the macula-disc center distance in mm (Pearson correlation coefficient, $r = -0.42$, $p = 0.09$).

The mean macula-disc center distance was 4.74 mm, SD 0.29 in Study III. No correlation was found between ametropia and the macula-disc center distance (Pearson correlation coefficient, $r = -0.07$, $p = 0.73$). The macula-disc center distance of subject 20, who was not included in the mean analysis but presented as a case report, was significantly longer than average (6.35 mm).

5.3 Dimension of the optic disc (III)

The dimensions of the optic disc in Study III were the following: mean width 1.72 mm, SD 0.11 and mean height 1.93 mm, SD 0.13. The width and height of the optic disc of subject 20 were 1.66 mm and 2.25 mm, respectively.

5.4 Correlation of relative change in the measured distance between two retinal vessel crossings with preoperative axial length, change in ametropia in D, and change in the anterior chamber depth in mm (II)

In Study II, the average change in ametropia induced by cataract surgery and IOL implantation was + 3.52 D, SD 6.86, and in the anterior chamber depth 0.89 mm (+27%), SD 0.57. The average change in axial length due to cataract surgery and IOL implantation was only -0.4 %, SD 0.002. This was considered to be insignificant. The average relative change in the measured distance between two retinal vessel crossings before and after surgery was -2.88 %, SD 0.02 measured using the fundus photographs taken with the telecentric Zeiss fundus camera. Relative change in the measured distance between two retinal vessel crossings measured using the fundus photographs taken with the telecentric Zeiss fundus camera correlated with change in ametropia in D (Pearson correlation coefficient, $r = -0.84$, $p = 0.01$). However, this result could not be repeated when subject 8, the subject with the most surgery induced change in ametropia (+19.13 D), was excluded from the analysis (Pearson correlation coefficient, $r = -0.56$, $p = 0.15$).

Neither change in the anterior chamber depth in mm nor preoperative axial length correlated significantly with relative change in the measured distance between two retinal vessel crossings measured using the fundus photographs taken with the Zeiss fundus camera (Pearson correlation coefficient, $r = 0.04$, $p = 0.93$ and $r = -0.42$, $p = 0.26$ respectively). In addition, the average change in the location of the second principal point P' from the apex of the cornea was -39.4% (SD 0.33) due to cataract surgery and IOL implantation.

5.5 Theoretical versus physiological location of the blind spot (I)

In Study I, the results of the 12 subjects examined with the Octopus custom made Blind spot visual field program were reliable. The reliability factor of the examination varied from 0.0 to 6.2 %. The theoretical location of the center of the blind spot of the 12 subjects examined corresponded to the location of the center of their physiological blind spot in the visual field (Table 1). The theoretical location of the center of the blind spot had a mean of 16.3°, SD 0.93, and the location of the center of the physiological blind spot had a mean of 15.3°, SD 1.15. The difference between these two locations had a mean of 0.96°, SD 1.18 (Table 1).

Table 1. Theoretical location of the center of the blind spot versus the location of the center of the physiological blind spot in degrees. The theoretical location of the center of the blind spot was calculated using the fundus photographs taken with the telecentric Zeiss fundus camera and the formula of Bennett et al. (1994). The location of center of the physiological blind spot was examined with the Octopus perimeter using a custom made Blind Spot visual field program. Adapted from Study I.

ID	Theoretical location of the blind spot (degrees)	Location of the physiological blind spot in the visual field (degrees)	Difference (degrees)	Spherical equivalent
2	17.1	16.5	0.5	-2.4
3	16.7	15.0	1.5	-0.5
4	16.6	16.0	0.5	-3.0
5	16.3	14.5	2.0	-2.0
6	17.2	15.5	1.5	-3.5
7	17.4	16.5	1.0	-0.8
9	14.8	13.0	2.0	-6.9
10	15.2	16.0	-1.0	-7.5
11	15.7	16.5	-1.0	-7.9
12	15.5	15.5	0.0	-5.0
13	15.8	13.5	2.5	+3.6
14	17.7	15.5	2.0	+1.5
Mean	16.3	15.3	0.96	
SD	0.93	1.15	1.18	

According to Bland-Altman plot (Bland & Altman 1986) the technique for calculating the theoretical location of the center of the blind spot based on fundus photography was in agreement with the results from the Octopus custom made Blind Spot visual field analysis used for determining the location of the center of the physiological blind spot. The mean difference between the two methods was 0.96° . This did not depend on the location of the blind spot. There was no systematic error between the measurements. In addition, there were no outliers. (Figure 12.)

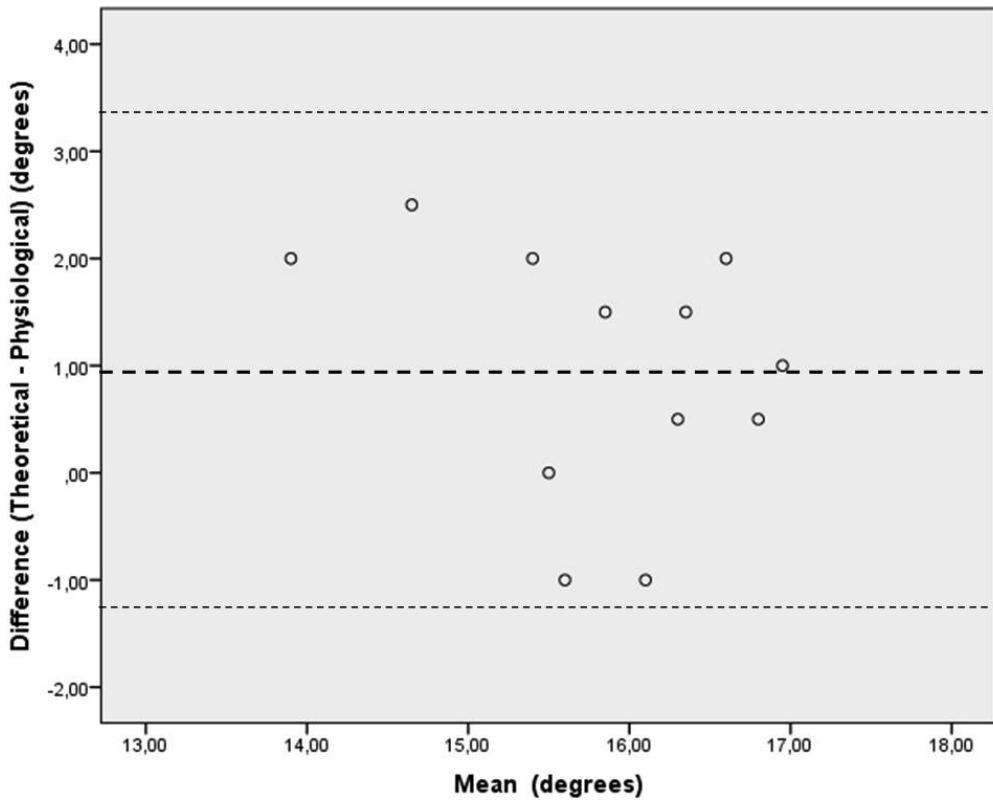


Figure 12. According to the Bland-Altman plot (Bland & Altman 1986) the technique for calculating the theoretical location of the center of the blind spot from fundus photographs was in agreement with the visual field examination based method for determining the location of the center of the physiological blind spot. The y-axis represents the difference between the two locations in degrees. The x-axis is the mean value of the two locations in degrees. The mean difference between the two locations was 0.96° , and did not depend on the location of the blind spot. The dotted line in the middle represents the mean difference of the two locations and the upper and the lower dotted lines represent the agreement interval. All of the differences between the two locations fall within this interval. There was no systematic error between the measurements. In addition, there were no outliers. Adapted from Study I.

5.6 Reaction times within and outside of the blind spot area in reaction time perimetry (IV)

Reaction times within the blind spot area of all the individuals studied were longer (mean 1751 ms vs. mean 987 ms) and showed more variability (SD 706 vs. 366) compared to other locations in the visual field. This difference was statistically significant in 10 of the 11 subjects, including subject 1 who only had a relative scotoma in the blind spot area determined using the Octopus custom made Blind Spot visual field program (Figure 13).

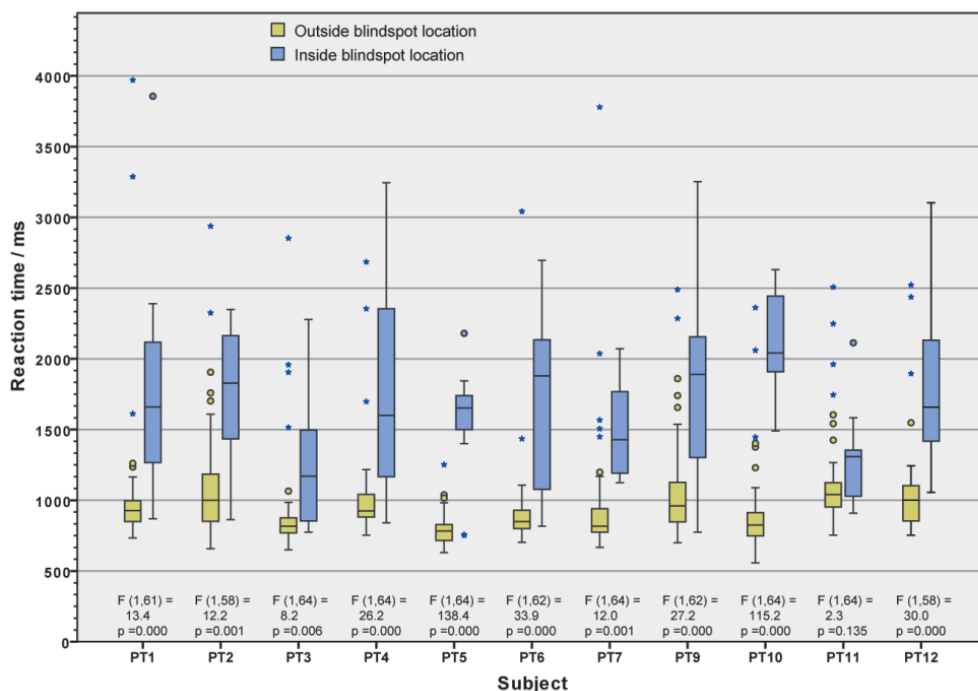


Figure 13. Box plot figure showing the reaction times of all the subjects. The reaction times within the blind spot area of all subjects examined except one (PT 11) were significantly longer than reaction times in other locations of the visual field. Adapted from Study IV.

6 DISCUSSION

6.1 Determining the size of retinal features (I and II)

Direct measurement of retinal features is only possible via vitreoretinal surgery. The problem with all the methods used for calculating the size of a retinal feature is that absolute exactness of the results will remain unattainable (Bengtsson & Krakau 1992). Garway-Heath et al. (1998) compared the reliability of the formula of Bennett et al. (1994) to other methods for calculating the size of a retinal feature and found it to be reliable.

The conclusion of Study I was that the theoretical location of the blind spot based on calculations carried out on fundus photographs using the formula of Bennett et al. (1994) corresponded to the location of the physiological blind spot determined by visual field examination with the Octopus custom made Blind Spot visual field program (Table 1). This further verifies that the formula of Bennett et al. (1994) offers a very close approximation of the true size of retinal features. This finding is in line with the work of Garway-Heath et al. (1998) where the reliability of the formula of Bennett et al. (1994) was also assessed. However, in Study I the method used to compare the theoretical location of the blind spot, based on calculations carried out on fundus photographs using the formula of Bennett et al. (1994), with the location of the physiological blind spot determined by the Octopus custom made Blind Spot visual field program also has its own flaws; this is due to the fact that the custom made Blind Spot visual field program is not immune to experimental error.

The mathematical basis of the formula of Bennett et al. (1994) is strongly founded in the unchanging laws of optics. However, it does include certain approximations (Bennett et al. 1994). It is clear that some uncertainty may be generated with each step when using the formula: Measurement error can occur when the size of a retinal feature from a fundus photograph and axial length are determined. Additional error may arise when the refractive index of the final ocular medium n is taken to be 1.336 in addition to accepting 1.82 mm as the location of the second principal point of the eye. Moreover, the process of taking a fundus photograph is not devoid of possible sources of error (Behrendt & Doyle 1965; Lotmar 1984; Pach et al. 1989). Furthermore, biology plays its own part and can cause aberrations and irregularities leading to possible additional uncertainty in the calculations. Hence, even at its best the formula of Bennett et al. (1994) is only an approximation of the truth.

In Study II, the effect of change in ametropia in D induced by cataract surgery and IOL implantation on the magnification of a fundus photograph taken with telecentric Zeiss and Topcon fundus cameras was studied. Any possible effect is important to take into

consideration because fundus photographs are used in the follow-up of many ocular diseases. Change in the size of an object can either be due to true growth or change in the magnification of a fundus photograph. The average relative change in the measured distance between two distinct retinal features, i.e., the same two retinal vessel crossings before and after surgery was small, only -2.88 %, SD 0.02 based on calculations carried out using the fundus photographs taken with the telecentric Zeiss fundus camera. Cataract surgery and IOL implantation caused no significant changes in axial length. Hence, only a small change between the pre and postoperative values was induced by the fact that the postoperative axial length was used in the calculations of the postoperative values.

In Study II, surgery induced relative change in the measured distance between two retinal vessel crossings based on calculations carried out using the fundus photographs taken with the telecentric Zeiss fundus camera correlated with change in ametropia in D (Pearson correlation coefficient, $r = -0.84$, $p = 0.01$). A negative correlation coefficient means that when there was a change in ametropia due to surgery from myopia towards emmetropia, this resulted in a negative change in the magnification of the fundus photograph, i.e., the post operative image was smaller than the preoperative image.

However, when subject 8 – the subject with the most surgery induced change in ametropia (+19.13 D) – was excluded from the analysis no statistically significant correlation was found (Pearson correlation coefficient, $r = -0.56$, $p = 0.15$). The relative change in the measured distance between two retinal vessel crossings of subject 8 was -7.2%. The weakness of the analysis is the small number of subjects enrolled. It is possible that by increasing the number of subjects enrolled a connection between smaller changes in ametropia and change in the magnification of the fundus photograph could be established. However, in a small sample study like this one, the inclusion of subject 8 – the one with the most change in ametropia in D (+19.13 D) – made the relative change in the measured distance between two vessel crossings statistically significant. Furthermore, the clinical relevance of a statistically significant finding still has to be evaluated separately. In Study II, the conclusion was that even the largest change in ametropia (+19.13 D in subject 8) only resulted in a small change in the magnification of the fundus photograph (-7.2%).

Even though the mathematical location of the post surgical P' was changed, on average -39.4%, SD 0.33, this has no clinically relevant effect on the magnification of the fundus photograph taken with the telecentric Zeiss fundus camera because the average change in the mathematical location of P' in mm is still very small ($-0.394 \cdot 1.82 \text{ mm} = -0.72 \text{ mm}$ in our work). Bennett et al. (1994) calculated the location of the second principal point P' of 12 individuals from the apex of the cornea based on their

personalized schematic eye models. The result was a variation of ± 0.55 mm from the accepted general value of P' (1.82 mm). This led to a total error of ± 0.007 in q since $0.01306 \cdot \pm 0.55 = \pm 0.007$. This is contrary to the unfortunate misquotation in Study I by the author, where the error calculated by Bennett et al. (1994) was stated to be 0.7%. In Study II, the average change of -0.72 mm in P' leads to a total error of -0.009 in q because $0.01306 \cdot -0.72 = -0.009$. This is close to the total error of ± 0.007 in q calculated by Bennett et al. (1994).

However, in Study II the calculations concerning the surgery induced change in the mathematical location of P' have an inherent error. First, the assumption that the preoperative mathematical location of P' equals 1.82 mm (Bennett et al. 1994) was made. It is nonetheless highly likely that a cataract may have affected this value preoperatively. The second assumption was that the true size of the preoperatively calculated distance between two retinal vessel crossings was correct. The postoperative location of P' was calculated based on these assumptions by substituting the calculated preoperative distance in the place of the variable t , and the corresponding measured postoperative distance in the place of the variable s in the formula of Bennett et al. (1994).

Even though the magnification of a fundus photograph and the mathematical location of P' can change in cataract surgery and IOL implantation, our data indicates that this leads to an error that is of no or at least only minor clinical significance when using the formula of Bennett et al (1994) in the calculations. Although the number of subjects enrolled in Study II was small the data further confirmed the use of the formula of Bennett et al. (1994). It can be used for calculating the true size of a retinal feature from a fundus photograph taken with a telecentric fundus camera after cataract surgery and IOL implantation. In addition, the results of Study II are in line with Study I, where the reliability of the formula of Bennett et al. (1994) was analyzed using healthy volunteers in a different clinical setting.

Our findings – together with the previous results of Bennett et al. (1994) and Garway-Heath et al. (1998) – give the scientific community great confidence to continue to apply, as it has for over twenty years, the formula of Bennett et al. (1994) in order to calculate the size of retinal features.

6.2 The conversion factor of the Topcon fundus camera (I and II)

According to Rudnicka et al. (1998) if a fundus camera is not telecentric by design, it prohibits the direct use of the formula of Bennett et al. (1994). In our Study I, little variation was found in the previously unknown conversion factor of the Topcon fundus camera (194.98 pixel/mm, SD 10.40 for a 50 degree lens). However, in the case of high

ametropia the use of nontelecentric imaging systems can lead to a significant amount of error in the magnification of a fundus photograph since the camera constant p can vary (Rudnicka et al. 1998). Care must be taken to avoid this possible error when making image size calculations on a fundus photograph of a subject with high ametropia when the optical properties of a given camera are not fully known.

In Study II, the mean pre and postoperative conversion factors of the Topcon fundus camera for a 50 degree lens were 185.47 pixel/mm, SD 12.36 and 183.27 pixel/mm, SD 13.92, respectively. Surgery induced relative change in the conversion factor of the Topcon fundus camera was analyzed and found to be small (only -1.19 %, SD 0.03). This was also the case with subject 8 (+0.43%), who had the most surgery induced change in ametropia (+19.13 D). No statistically significant correlation was found between the relative change of the conversion factor of the Topcon and change in ametropia in D (Pearson correlation coefficient, $r = -0.17$, $p = 0.66$). This led to the conclusion that fundus photography with the Topcon fundus camera is reliable after cataract surgery and IOL implantation even in cases where the ametropia is changed due to surgery.

6.3 Macula-disc center distance (I and III)

The results of Study I support the previous findings that there is little variation in the macula-disc center distance in mm between adults. It can be used as a reference tool in order to determine the size of retinal features on fundus photographs (Bartling et al. 2008). The macula-disc center distance in Study I was 4.73 mm, SD 0.29. Mok and Lee (2002) and Bartling et al. (2008) have found the macula-disc center distance to be 4.69 mm, SD 0.08 and 4.62 mm, SD 0.33, respectively. The results of Hong et al. (2010) stated 4.503 mm, SD 0.373 in the right eye and 4.458 mm, SD 0.376 in the left eye. Study I supported the previous findings of Bartling et al. (2008): the macula-disc center distance was close to a constant and thus can be used as an internal reference tool when estimating the size of an object from fundus photographs taken with a nontelecentric fundus camera when the optical principals behind the camera used are not known.

However, ocular pathology may potentially affect measurements carried out on fundus photographs. In the work of Hellström et al. (1997) ocular fundus morphology was evaluated in preterm children whose mean postmenstrual gestational age was 29.1 weeks. They found no difference in optic disc morphology between preterm children and control subjects. In another study by Hellström et al. (2000) ocular fundus abnormalities were described in children born before 29 weeks of gestation. They found that preterm birth was associated with subnormal optic disc and rim areas.

In our Study III, the effect of premature birth on the anatomy of the posterior pole was assessed by measuring the macula-disc center distance of prematurely born children aged 10 – 11 years. Little variation was found in the macula-disc center distance of these prematurely born children (mean 4.74 mm, SD 0.29). Hence, also in prematurely born children aged from 10 to 11 years, it provides an easy-to-use reference tool for evaluating the size of retinal features from fundus photographs. The Optic-Disc-to-Fovea Distance (ODF; equivalent to the macula-disc center distance) in preterm and full-term infants has previously been studied by De Silva et al. (2006). In their study, the postmenstrual age ranged from 32 to 50 weeks. The mean ODF was 4.4 mm, SD 0.4. They discussed the fact that the growth of the highly organized area of the posterior pole appears limited (11 %) from birth to adulthood. This result was also supported by our study.

Furthermore, in Study III the macula-disc center distance of subject 20, who was diagnosed with ROP, was significantly longer than average (6.35 mm). The ROP itself or high myopia associated with it are possible causes for the axial length to be longer than average (the spherical equivalent of the left eye of subject 20 was -20.50 D and axial length 25.64 mm). The effect of possible macular dragging due to ROP could not be ruled out, although no retinal folds were detected. In addition, no staphyloma was present.

Previously, no correlation has been found between the macula-disc center distance and ametropia (Bartling et al. 2008). In the work of Bartling et al. (2008), the range of ametropia was only from -9 to +6 D. However, this finding was supported by the results of Study III where no correlation was found between ametropia and the macula-disc center distance ($r = -0.07$, $p = 0.73$).

Another difference in subject 20 was the shape of the disc, which was vertically oval. In adult eyes, the average dimensions of the optic disc are: width 1.77 mm, SD 0.19 and height 1.88 mm, SD 0.19 (Quigley et al. 1990). Previously, in adult eyes a longer axial length has been shown to associate with a longer distance between the disc and foveola, a larger index of ovalness, and a larger disc ($P < 0.01$) (Chihara & Chihara 1994).

However, all the calculations concerning subject 20 in Study III may have involved an inherent source of error, since the mean conversion factor of the Topcon fundus camera used (194.98 pixel/mm, SD 10.40 for a 50 degree lens) might not apply in the case of high ametropia.

ROP and other ocular pathology can affect physiological retinal features, and thus potentially alter the results of the measurements carried out on fundus photographs. In cases of high ametropia and macular dragging the macula-disc center distance might

vary from the average. Hence, a personal macula-disc center distance should be determined and used as a refined reference tool for determining the size of retinal features using fundus photographs instead of relying on average dimensions.

The personal macula-disc center distance in degrees can be determined by studying the location of the center of the physiological blind spot of the subject in question using a perimeter, and then by dividing the result with the refractive index of the final ocular medium (1.336). The personal macula-disc center distance in degrees can then be used as a refined reference tool in order to determine the size of retinal features. In addition, it can further be converted into metric units by using the Equation 14 if the axial length is known.

The limitation of the Equation 14, like that of the Equation 3, is that it is a simplified method for calculating U' . However, it was chosen for its applicability. In using the Equation 14 an assumption that the length of P'D is equal to P'M is made (Figure 10). From this follows that $U' = t / k'$ when U' is expressed in radians (Equation 3). However, this can add some error. We calculated the error in U' when using the Equation 14 in an average eye of 22 mm axial length and 4.7 mm macula-disc center distance and found it to be small (2.6 %).

6.4 Reaction time perimetry (IV)

In Study IV, the results from Study I were used for reference: First, the Octopus custom made Blind Spot visual field program for detecting the location of the physiological blind spot. Second, fundus photography with the telecentric Zeiss fundus camera for calculating the location of the theoretical blind spot using the formula of Bennett et al. (1994). The results from these two independent methods corresponded with each other. The results of the Octopus custom made Blind Spot visual field program were chosen to define the location of the center of the physiological blind spot.

The reaction times for detecting the STS displayed within the physiological blind spot area measured with the reaction time perimeter of all the individuals except one (subject 11) were longer than for stimuli displayed within other locations of the visual field (mean 1751 ms, SD 706 vs. mean 987 ms, SD 366 respectively). Hence, the results were able to show that the reaction time perimeter is capable of finding a physiological scotoma, i.e., the blind spot.

There are a few possible reasons why the reaction time perimeter was unable to find the blind spot of subject 11. First, the predetermined location of the blind spot could be incorrect, although this is highly unlikely because there were two independent methods for determining its center (Table 1). Second, most of the blind spot of subject 11 was

located just below meridian 8° , the one used in Study IV. The upper border of the part of the blind spot that was completely blind was just barely touching this meridian in subject 11. The most logical explanation for not finding any statistically significant difference in the reaction times of subject 11 within and outside of the blind spot area is that the location considered to be blind was not blind enough or not blind at all.

The data in Study IV indicates that shorter reaction times and also smaller variability for stimuli displayed outside of the blind spot area result from a reflex saccade that is initiated by the recognition of the STS in the peripheral visual field. This allows for a rapid turning of the eyes towards the STS and visualization of the FO with the fovea. When a peripheral stimulus is displayed within the blind spot area, and therefore not seen, the subject is forced to perform a visual search for the FO. However, depending on the location of the FO and the direction of the first saccade(s), it is possible that occasionally by chance, the FO can be detected rapidly. Furthermore, it is possible that sometimes learning from previous experience can affect the time needed to search for the FO. In Study IV, the FO was always located at the temporal visual field when the STS was not seen, and thus learning from previous experience can speed up the search for it.

7 SUMMARY AND CONCLUSIONS

The following are the main findings of this thesis:

1. The formula of Bennett et al. (1994) for determining the size of retinal features was verified using healthy volunteers by first measuring the macula-disc center distance from fundus photographs taken with the telecentric Zeiss fundus camera, and then by calculating the theoretical location of the blind spot based on the macula-disc center distance. These results were found to correspond to the results from visual field examination using the Octopus custom made Blind Spot visual field program where the location of the physiological blind spot was determined. Thus, the formula of Bennett et al. (1994) was considered to be reliable within the ametropia range used (from -7.88 to +3.63 D).
2. The effect of change in ametropia in D caused by cataract surgery and IOL implantation on the magnification of a fundus photograph taken with the telecentric Zeiss fundus camera was found to be small (average -2.88 %, SD 0.02). Change in ametropia in D and the relative change in the measured distance between two retinal vessel crossings measured from fundus photographs taken before and after surgery had a statistically significant correlation only when subject 8 – who had the most change in ametropia (+19.13 D) – was included in the analysis (Pearson correlation coefficient, $r = -0.84$, $p = 0.01$).
3. The magnification characteristics of the Topcon fundus camera were assessed, and the change in ametropia after cataract surgery and IOL implantation was found to have a non-significant effect on the conversion factor of the Topcon fundus camera.
4. The macula-disc center distance of prematurely born children aged from 10 to 11 years was calculated. The macula-disc center distance was found to be close to a constant. Hence, it was concluded that it could be used as a reference tool for determining the size of retinal features from fundus photographs.
5. A novel method – the reaction time perimeter – was introduced. The reaction time perimeter was shown to be able to detect the physiological blind spot. Validating the use of reaction time perimetry for examining the visual field in different ocular pathology requires further studies.

8 FUTURE DIRECTIONS

8.1 The use of the formula of Bennett et al. (1994) after cataract surgery and IOL implantation (II)

The primary intention of this study was to discover if change in ametropia caused by cataract surgery and IOL implantation induces a significant change in the magnification of a fundus photograph taken with the telecentric Zeiss and Topcon fundus cameras. Therefore, the original design was to enroll a group of subjects that would represent a wide field of surgery induced change in ametropia in D. In Study II, technical difficulties were encountered which caused the number of subjects enrolled to be small.

A greater number of subjects are needed in order to further analyze the effect of change in ametropia in D after cataract surgery and IOL implantation on the magnification of a fundus photograph taken with the telecentric Zeiss fundus camera. However, as the expected change is very small, the number of subjects enrolled would have to be very large. In light of the fact that the clinical relevance of finding such a small change in the magnification of a fundus photograph is most likely going to be negligible, it is necessary to question the benefit to be gained from planning such a study.

8.2 Reaction time perimetry (IV)

We hypothesize that in the future reaction time perimetry can offer advantages compared to standard automated perimetry. The advantage of the reaction time perimeter is that it allows physiological visual reflexes to direct gaze towards the peripheral STS in order to detect the FO with the fovea. Hence, the need to maintain a prolonged stable fixation is not required, and thus makes reaction time perimetry a simplified simulation of real life viewing.

Different individuals within a similar subgroup of subjects may have a diverse result profile in reaction time perimetry. Some may proceed at a faster pace than others when the STS is seen, and some may have to take a significantly longer time than others to search for the FO when the STS is not seen. In further studies, these possible physiological differences between individuals should be taken into consideration.

In the future, reaction time perimetry may demonstrate a greater power in predicting the impact of disease on the ability to perform the activities of daily living compared to SAP. However, further research is needed to gain knowledge of the advantages and disadvantages of using the novel reaction time perimeter for visual field analysis.

9 ACKNOWLEDGEMENTS

The present work was carried out at the Department of Ophthalmology, Turku University Hospital. I want to express my deepest gratitude to professor Eija Vesti. Eija has been an invaluable tutor and mentor, always willing to help me with everything.

I want to thank my supervisor doctor Markku Leinonen for introducing me to his novel invention, the reaction time perimeter. Without Markku's help and guidance, it would not have been possible to finish this thesis.

I also wish to thank docent Eero Aarnisalo for introducing me into the world of ophthalmology and for being the first person to mentor me when I first became interested in the magnification of a fundus photograph. The brilliant mind of Eero has greatly shaped the original idea of this thesis.

I deeply thank adjunct professor Olavi Pärssinen and associate professor Juha Toivonen for their valuable and constructive criticism. Both of these gentlemen played a vital part in making this thesis a better one. Olavi especially really put his mind and considerable effort into the work and found most of my typos among many other corrections.

I thank Tuomo Lehtonen for providing me with the fundus photographs of prematurely born children in Study III and also for enrolling the subjects in Study II.

I would like to thank Mr. Kari Nummelin for the fundus photography, and Mrs. Vappu Keppola and other personnel working at the Turku University Hospital for their assistance.

I am deeply grateful to Mrs. Sinikka Vuorela – my dear neighbor – for helping me with most of the images in this thesis.

I deeply thank my parents Ritva and Pekka for all their support over the years. I want to thank my dear Father Pekka for his comments concerning my thesis.

Lastly, I want to thank my loving husband Jonni for always being there for me and for providing me with such joy and comfort.

This thesis was supported financially by the following funds and foundations: Nissin säätiö, Kaukomarkkinat Oy, the Finnish Ophthalmological Society, the University of Turku, Hilda Kauhasen muistosäätiö, TYKS-säätiö, Lääketieteen säätiö. The author reports no conflict of interest.

Rauma, April 2018

Laura Knaapi

10 REFERENCES

- American Academy of Ophthalmology (2005): *Clinical Optics 2005–2006*. 1st ed. San Francisco, Calif.
- Arnold JV, Gates JWC & Taylor KM (1993): Possible errors in the measurement of retinal lesions. *Invest Ophthalmol Vis Sci* **34**:2576–2580.
- Bakaraju RC, Ehrmann K, Papas E & Ho A (2008): Finite schematic eye models and their accuracy to in-vivo data. *Vision Res* **48**:1681–1694.
- Bartling H, Wanger P & Martin L (2008): Measurement of optic disc parameters on digital fundus photographs: algorithm development and evaluation. *Acta Ophthalmol* **86**:837–841.
- Behrendt & Doyle (1965): Reliability of image size measurements in the new Zeiss fundus camera. *Am J Ophthalmol* **59**:896–899.
- Bengtsson B & Krakau CET (1977): Some essential features of the Zeiss fundus camera. *Acta Ophthalmol* **55**:123–131.
- Bengtsson B & Krakau CET (1992): Correction of optic disc measurements on fundus photographs. *Graefes Arch Clin Exp Ophthalmol* **230**:24–28.
- Bennett AG, Rudnicka AR & Edgar DF (1994): Improvements on Littmann's method of determining the size of retinal features by fundus photography. *Graefes Arch Clin Exp Ophthalmol* **232**:361–367.
- Bland JM & Altman DG (1986): Statistical methods for assessing agreement between two methods of clinical measurement. *Lancet* **1**:307–310.
- Chihara E & Chihara K (1994): Covariation of optic disc measurements and ocular parameters in the healthy eye. *Graefes Arch Clin Exp Ophthalmol* **232**: 265–271.
- Coleman AL, Haller JA, Quigley HA (1996): Determination of the real size of fundus objects from fundus photographs. *J Glaucoma* **5**:433–435.
- De Almeida MS & Carvalho LA (2007): Different Schematic Eyes and their Accuracy to the in vivo Eye: A Quantitative Comparison Study. *Braz J Phys* **37**: 378–387.
- De Silva JD, Cocker KD, Lau G, Clay ST, Fielder AR & Moseley MJ (2006): Optic Disk Size and Optic Disk-to-Fovea Distance in Preterm and Full-Term Infants. *Invest Ophthalmol Vis Sci* **47**:4683–4686.

- Garway-Heath DF, Rudnicka AR, Lowe T, Foster PJ, Fitzke FW & Hitchings RA (1998): Measurement of optic disc size: equivalence of methods to correct for ocular magnification. *Br J Ophthalmol* **82**:643–649.
- Hellström A, Hård AL, Chen Y, Niklasson A & Albertsson-Wikland K (1997): Ocular fundus morphology in preterm children. Influence of gestational age, birth size, perinatal morbidity, and postnatal growth. *Invest Ophthalmol Vis Sci* **38**: 1184–1192.
- Hellström A, Hård A-L, Svensson E & Niklasson A (2000): Ocular fundus abnormalities in children born before 29 weeks of gestation: a population-based study. *Eye* **14**: 324–329.
- Hong SW, Ahn MD, Kang SH & Im SK (2010): Analysis of Peripapillary Retinal Nerve Fiber Distribution in Normal Young Adults. *Invest Ophthalmol Vis Sci* **51**:3515–3523.
- <http://ecee.colorado.edu/~mcleod/pdfs/OESD/lecturenotes/ThickLenses.pdf> (accessed March 10, 2018)
- <http://imagej.nih.gov/ij/> (accessed March 10, 2018)
- <http://www.opto-engineering.com/resources/telecentric-lenses-tutorial> (accessed March 10, 2018)
- Kanski JJ & Kubicka-Trzaska A (2007): *Clinical Ophthalmology*. 6th ed. Edinburgh: Elsevier Churchill Livingstone.
- Katz J & Sommer A (1988): Reliability indexes of automated perimetric tests. *Arch Ophthalmol* **106**:1252–1254.
- Knaapi L, Aarnisalo E, Vesti E & Leinonen MT (2015): Clinical verification of the formula of Bennett et al. (1994) of determining the size of retinal features by fundus photography. *Acta Ophthalmol* **93**: 248–252.
- Knaapi L, Lehtonen T, Vesti E, Leinonen MT (2015): Determining the size of retinal features in prematurely born children by fundus photography. *Acta Ophthalmol* **93**: 339–41.
- Knaapi L, Vesti E, Leinonen MT (2015): Detecting the Physiological Blind Spot with Reaction Time Perimeter. *J Clin Exp Ophthalmol* **6**:493. doi:10.4172/2155-9570.1000493
- Knaapi L, Lehtonen T & Vesti E (2017): The effect of cataract surgery and IOL implantation on the magnification of a fundus photograph: a pilot study. *Acta Ophthalmol* **95**: 839–841.
- Littmann H (1955): Die Zeiss-Funduskamera. *Ber Dtsch Ophthalmol Ges* **59**:318–21.
- Littmann H (1982): Zur Bestimmung der wahren Größe eines Objektes auf dem Hintergrund des lebenden Auges. *Klin Monbl Augenheilkd* **180**:286–289.

- Littmann H (1988): Zur Bestimmung der wahren Größe eines Objektes auf dem Hintergrund des lebenden Auges. *Klin Monbl Augenheilkd* **192**:66–67.
- Lotmar W (1984): Dependence of magnification upon the camera-to-eye distance in the Zeiss fundus camera. *Acta Ophthalmol* **62**:131–134.
- McKean-Cowdin R, Varma R, Wu J, Hays RD & Azen SP (2007): Severity of Visual Field Loss and Health-related Quality of Life. *Am J Ophthalmol* **143**:1013–1023.
- Meyer JH, Guhlmann M & Funk J (1997): Blind spot size depends on the optic disc topography: a study using SLO controlled scotometry and the Heidelberg retina tomograph. *Br J Ophthalmol* **81**:355–359.
- Meyer T & Howland HC (2001): How large is the optic disc? Systematic errors in fundus cameras and topographers. *Ophthalmic Physiol Opt* **21**:139–150.
- Mok KH & Lee VW (2002): Disc-to-macula distance to disc-diameter ratio for optic disc size estimation. *J Glaucoma* **11**:392–395.
- Pach J, Pennell DO, Romano PE (1989): Optic disc photogrammetry magnification factors for eye position, centration, and ametropias, refractive and axial; and their application in the diagnosis of optic nerve hypoplasia. *Ann Ophthalmol* **21**:454–462
- Quigley HA, Brown AE, Morrison JD & Drance SM (1990): The size and shape of the optic disc in normal human eyes. *Arch Ophthalmol* **108**:51–57.
- Quigley MG & Dubé P (2003): A new fundus camera technique to help calculate eye-camera magnification: A rapid means to measure disc size. *Arch Ophthalmol* **121**:707–709.
- Racette L, Fischer M, Bebie H, Holló G, Johnson CA, Matsumoto C (2016): *Visual Field Digest: A guide to perimetry and the Octopus perimeter*. 6th ed. pdf
- Richman J, Lorenzana LL, Lankaranian D, Dugar J, Mayer JR, Wizov SS & Spaeth GL (2010): Relationships in Glaucoma Patients Between Standard Vision Tests, Quality of Life, and Ability to Perform Daily Activities. *Ophthalmic Epidemiol* **17**:144–151.
- Rudnicka AR, Edgar DF, Bennett AG (1992): Construction of a model eye and its applications. *Ophthalmic Physiol Opt* **12**:485–490.
- Rudnicka AR, Burk RO, Edgar DF & Fitzke FW (1998): Magnification characteristics of fundus imaging systems. *Ophthalmology* **105**:2186–2192.
- Tatham AJ, Boer ER, Rosen PN, Penna M Della, Meira-Freitas D, Weinreb RN, Zangwill LM & Medeiros FA (2014): Glaucomatous Retinal Nerve Fiber Layer Thickness Loss Is Associated With Slower Reaction Times Under a Divided Attention Task. *Am J Ophthalmol* **158**:1008–1017.

Tschopp C, Safran AB, Viviani P, Bullinger A, Reicherts M & Mermoud C (1998): Automated visual field examination in children aged 5–8 years. Part I: Experimental validation of a testing procedure. *Vision Res* **38**:2203–2210.

Wilms KH (1986): Zur Struktur einfacher Programme zur Berechnung von absoluten Grossen des Augenhintergrundes. *Optometrie* **4**:204–206.

Yanoff M & Duker JS (2009): *Ophthalmology*. 3rd ed. London: Mosby

Annales Universitatis Turkuensis



Turun yliopisto
University of Turku

ISBN 978-951-29-7307-1 (PRINT)
ISBN 978-951-29-7308-8 (PDF)
ISSN 0355-9483 (PRINT) | ISSN 2343-3213 (PDF)